Measurement Report: Four-year Variability and Influence of Winter Olympics and other Special Events on Air Quality in Urban Beijing during Wintertime

Yishuo Guo[1,2,★], Chenjuan Deng[3,2,★], Aino Ovaska[2], Feixue Zheng[1], Chenjie Hua[1], Junlei Zhan[1], Yiran Li[3], Jin Wu[3], Zongcheng Wang[1], Jiali Xie[1], Ying Zhang[1], Tingyu Liu[1], Yusheng Zhang[1], Boying Song[1], Wei Ma[1], Yongchun Liu[1], Chao Yan[4,1,2], Jingkun Jiang[3], Veli-Matti Kerminen[2], Men Xia[2,1], Tuomo Nieminen[2], Wei Du[2,1,*], Tom Kokkonen[2,1,4,*], Markku Kulmala[1,2]

[1] Aerosol and Haze Laboratory, Beijing Advanced Innovation Center for Soft Matter Science and Engineering, Beijing University of Chemical Technology, Beijing, China

[2] Institute for Atmospheric and Earth System Research / Physics, Faculty of Science, University of Helsinki, Finland

[3] State Key Joint Laboratory of Environment Simulation and Pollution Control, State Environmental Protection Key Laboratory of Sources and Control of Air Pollution Complex, School of Environment, Tsinghua University, Beijing, China

[4] Joint International Research Laboratory of Atmospheric and Earth System Research, School of Atmospheric Sciences, Nanjing University, Nanjing, China

★ These authors contributed equally to this work.

* *Correspondence to:* Wei Du (wei.du@helsinki.fi) and Tom Kokkonen (tom.kokkonen@helsinki.fi)

Abstract. Comprehensive measurements are vital to obtain big enough datasets for better understanding the complex atmosphere and further improving the air quality. To investigate the four-year variation of air quality and the influences of special events (Beijing Winter Olympics, COVID lockdown and Chinese New Year) on it during the wintertime in polluted urban air, we conducted comprehensive observations in Beijing, China, during January 1st – February 20th, in the years from 2019 to 2022. The mass concentration of $PM_{2.5}$ and its composition (organics, nitrate, sulfate, ammonium, chloride and black carbon), number size distributions of particles (down to ~1 nm) and ions, gaseous pollutants (CO, NO_x, SO_2, O_3), condensable vapors (sulfuric acid and oxygenated organic molecules), as well as meteorological parameters were simultaneously measured. The days before January 22nd without any special event in each year were selected to investigate the four-year variability of air quality. We found that the concentrations of CO, NO_x, total oxygenated organic molecules (OOMs), total $PM_{2.5}$, organics, chloride, black carbon and the number concentration of sub-3 nm particles ($N_{1.3-3}$) showed similar variations, decreasing from 2019 to 2021 and then increasing in 2022. For SO_2, however, its concentration decreased year by year due to the significant emission reduction, further leading to the decrease of gaseous sulfuric acid and particulate sulfate from 2019 to 2022. O_3 concentration showed an opposite four-year variation compared with NO_x. Meanwhile, both the oxygen and nitrogen contents of oxygenated organic molecules increased year by year, implying that not only the oxidation state of those compounds increased, but also NO_x was involved more efficiently in their formation processes. With higher sulfuric acid concentrations and NPF frequencies in 2021 than in 2022, and with the lowest concentrations of background aerosols and the lowest ambient temperatures in 2021, $N_{1.3-3}$ was still the lowest in 2021. Unlike $N_{1.3-3}$, the ion concentrations in both 0.8-2 and 2-4 nm size ranges were higher in 2021 than in the other years. Then, the days after 4th February were chosen to explore the influence of special events. The non-event days within this date range in 2019 and 2021 was chosen as the Reference period. Due to the favorable meteorological conditions together with reductions in anthropogenic emissions, there were basically no haze events during the Olympics. Therefore, CO, NO_x, SO_2, total OOMs, accumulation mode particles ($N_{100-1000}$), total $PM_{2.5}$ and its compositions were much lower, while ion concentrations were much higher compared with the Reference period. Although there was also emission reduction during the COVID, especially for NO_x, the enhancement of secondary inorganic aerosol formation, together with unfavorable meteorological conditions, caused severe haze events during this period. Hence, CO, total OOMs and all $PM_{2.5}$ compositions during the COVID increased dramatically compared with the Reference period. Influenced by SO_2, condensation sink and sunlight, sulfuric acid concentration was found to be comparable between Olympics and the

Reference period, but was lower during COVID and Chinese New Year. Additionally, $N_{1.3\text{-}3}$ was almost at the same level during different periods, indicating that the special events only had little impacts on the new particle formation processes. These results provide useful information to the development of more targeted pollution control plans.

1. Introduction

Beijing and the surrounding areas suffer from poor air quality associated with high particulate matter (PM) concentrations, especially during wintertime. To improve the air quality, extensive studies have been carried out to understand the sources, formation and evolution of air pollutants in Beijing (An et al., 2019;Sun et al., 2014;Zheng et al., 2015;Shang et al., 2020;Cheng et al., 2016). Primary emission sources, including traffic, cooking, coal combustion and biomass burning, have been identified (Du et al., 2022b;Cai et al., 2020;Liu et al., 2016b). Of primary emissions, those from combustions were found to be the major contributors to haze, especially during the heating season (Cheng et al., 2013;Sun et al., 2013b;Sun et al., 2014).

Compared with primary emissions, secondary aerosols have been shown to play a more important role on haze formation, with contributions higher than 60% of PM_1 mass concentration in Beijing (Shang et al., 2020;Huang et al., 2014;Kulmala et al., 2022). Secondary organic aerosols (SOA), nitrate (NO_3) and sulfate (SO_4) originate from their gaseous precursors, e.g., volatile organic compounds (VOCs), nitrogen oxides (NO_x), and sulfur dioxide (SO_2). VOCs, NO_x, and SO_2 further produce oxygenated organic molecules (OOMs), nitric acid (HNO_3), and sulfuric acid (H_2SO_4), respectively, via homogeneous reactions, which can contribute to particle growth by condensation (Bianchi et al., 2019;Wang et al., 2020b;Trostl et al., 2016;Yue et al., 2010). Most recently, Nie et al. (2022) reported that the condensation of OOMs contributed to >30% of SOA in Beijing. Meanwhile, heterogeneous reactions were found to promote the formation of secondary aerosols. Dissolved SO_2 can be oxidized into SO_4 by atmospheric oxidants, e.g., H_2O_2, O_3, and NO_2 (Zhang et al., 2015;Wang et al., 2020a;Cheng et al., 2016). Heterogeneous reactions between HNO_3 and NH_3 in daytime, and hydrolysis of N_2O_5 during night-time are the main pathways forming NO_3 (Xue et al., 2014;Wang et al., 2017). Furthermore, liquid-phase related SOA were found to increase during severe haze when relatively humidity was high (Xu et al., 2017;Zhao et al., 2019). These results highlight the importance of reducing, not only the primary particulate emissions, but also the anthropogenic gaseous precursors to suppress secondary aerosol formation in regional scales (Kulmala et al., 2020;Du et al., 2021).

Regional transport and meteorological conditions also play roles on the evolution of haze episodes. Air masses coming from the south of Beijing often bring pollutants to this area, and hence favor the rapid built up of particle masses (Ma et al., 2017;Zheng et al., 2015;Sun et al., 2015). It has been found that 40% of $PM_{2.5}$ could originate from regional transport in an annual scale (Ge et al., 2018), and under very unfavorable meteorological conditions, it could contribute even up to 80% of the total particle mass during a single haze episode (Sun et al., 2016). Besides, haze events occur typically under stagnant conditions (Zheng et al., 2015). Under such circumstance, high aerosol concentrations tend to delay the onset of precipitation (Guo et al., 2016), and thus, the relative humidity (RH) within the boundary layer is often rather high, which further promotes the heterogeneous reactions producing secondary aerosols (Sun et al., 2013a). Additionally, results have shown that when RH increased above 60%, particles were found to be in a liquid state, thereby accelerating secondary formation (Liu et al., 2017).

The air quality in Beijing has improved substantially over the past decade, especially after introducing the "Action Plan for Air Pollution Prevention and Coontrol" in 2013 (Wang et al., 2020d;Lu et al., 2020;Li et al., 2020b). However, the particulate pollution in Beijing still exceeds the national air quality standards (Xiao et al., 2020). Besides, although the concentration of SO_2 decreased significantly, the level of NO_x remains still high, which results in NO_3 becoming the main contributor of secondary inorganic aerosols (SIA) (Xie et al., 2020). Furthermore, concurrent with the decreasing PM concentrations, ozone is rapidly becoming a year-round air pollution problem in China (Li et al., 2021).

In addition to long-term actions, Beijing has imposed strict short-term emission reductions during highly visible international events, such as Beijing Summer Olympics in 2008 (Wang et al., 2010;Shou-bin et al., 2009;Okuda et al., 2011;Schleicher et al., 2012), Asia – Pacific Economic Conference (APEC) in 2014 (Chen et al., 2015;Sun et al., 2016), and Victory Day Parade in 2015 (Zhao et al., 2017). More recently, after the start of the COVID-19 outbreak, the Chinese government carried out strong restrictions (COVID lockdown) in order to prevent the spread of virus. Reduced anthropogenic activities resulted in decreased emissions, yet severe pollution episodes were still observed (Le et al., 2020). In preparation for the Beijing Winter Olympics, the Chinese government authorized necessary actions, successfully improving air quality during this period. Additionally, annual Chinese New Year celebrations are typically associated with reductions in anthropogenic emissions during the 7-day holiday (Tan et al., 2009;Lin and McElroy, 2011).

All those special events mentioned above have different characteristics in regard to emission reductions. During the COVID lockdown, traffic was reduced, but cooking emissions and industrial activities continued at least partially (Shi and Brasseur, 2020). During the Beijing Winter Olympics, heavy industrial activities were regulated to improve the air quality. During the Chinese New Year, a large proportion of Beijing migrant workers and students from other cities are leaving the city and returning to their hometown. Therefore, anthropogenic emissions from e.g., traffic, cooking and industry are reduced substantially. Thus, a comparison between COVID lockdown, Beijing Winter Olympics and Chinese New Year can provide a unique chance to investigate the response of air pollutants to different emission reduction actions.

In this study, we examined the wintertime (1st January to 20th February) air quality in urban Beijing during a four-year period from 2019 to 2022. We utilised comprehensive observations of air pollutants in both gas phase (including carbon monoxide, sulfur dioxide, nitrogen oxides, ozone, sulfuric acid, and oxygenated organic molecules) and particle phase (including number size distributions of particles and ions, mass concentrations of $PM_{2.5}$ and its compositions), as well as of meteorological conditions (including temperature, RH, UVB radiation, wind speed and direction, and boundary layer height) from Aerosol and Haze Laboratory operated by Beijing University of Chemical Technology (AHL-BUCT; Liu et al., 2020). The objectives of this study are 1) to investigate the four-year variabilities of different pollutants and to understand their connections with emissions and meteorological conditions, and 2) to examine the characteristics of atmospheric pollution cocktail during different short-term special events (Beijing Winter Olympics, COVID lockdown and Chinese New Year periods) associated with substantial emission reductions. This study provides helpful information on pollution characteristics of urban Beijing both in a long-term scale and short-term special periods with different emission reductions, which can give guidance to make targeted and sustainable emission control plans.

2. Measurements and methods

2.1 Site description

Beijing is located in the northwestern part of the North China Plain. There are two mountains and a sea nearby. The Taihang Mountain is to the west and the Yanshan Mountain is to the northwest of Beijing, and the nearest Bohai Sea is ~ 150 km to the east. On the south of Beijing, there are several megacities, such as Baoding and Shijiazhuang. Our measurements were conducted at downtown Beijing, the west campus of Beijing University of Chemical Technology (39.95° N, 116.31° E). The instruments are located on the fifth floor of a teaching building, which is ~ 20 m above the ground level. The station can be

considered as a representative urban site, and more detailed information can be found elsewhere (Liu et al., 2020;Yan et al., 2021;Guo et al., 2021;Du et al., 2022a).

120 **2.2 Instrumentation**

Meteorological variables were measured with a weather station (AWS310, Vaisala Inc.) located on the rooftop of the building. The boundary layer height (BLH) was measured using a ceilometer (CL51, Vaisala). Mixing ratios of trace gases, including carbon monoxide (CO), sulfur dioxide (SO_2), nitrogen oxides (NO_x) and ozone (O_3), were monitored using Thermo Environmental Instruments (models 48i, 43i-TLE, 42i, 49i, respectively).

125 The concentrations of neutral sulfuric acid (SA) and oxygenated organic molecules (OOMs) were measured by a chemical ionization atmospheric pressure interface long-time-of-flight (CI-APi-TOF, Aerodyne Research, Inc.) mass spectrometers using nitrate (NO_3^-) as the reagent ion. Detailed configurations and working parameters of this nitrate CIMS can be found elsewhere (Yan et al., 2022;Guo et al., 2022). The calibration of SA was implemented by introducing a known amount of gaseous SA produced by the reaction of SO_2 and OH radical formed by UV photolysis of water vapor, which is similar to the

130 method in previous literatures (Kürten et al., 2012). The calibration factor of sulfuric acid was $6.07 - 7.47 \times 10^9$ cm^{-3} / (normalized cps) from 2019 to 2022. For the quantification of OOMs, a mass-dependent transmission method was used and details of this approach is described elsewhere (Heinritzi et al., 2016). The concentration of each molecular OOM species is calculated as follows:

$$[OOM] = \frac{\sum_{i=0}^{1}(OOM)(HNO_3)_i NO_3^- + (OOM-H)^-(HNO_3)_i}{\sum_{i=0}^{2}(HNO_3)_i NO_3^-} \times C \div T_{OOM} \qquad (1)$$

135 where [OOM] is the concentration of one specific OOM molecule, the numerator on the right-hand side is the sum of detected signal of that OOM, either as neutral molecule or as de-protonated ion (OOM-H)$^-$, the denominator is the sum of all measured reagent ions, C is the calibration factor of H_2SO_4 and T_{OOM} is the relative transmission coefficient.

The mass concentration of $PM_{2.5}$ was measured with a Tapered Element Oscillating Microbalance Dichotomous Ambient Particulate Monitor (TEOM 1405-DF, Thermo Fisher Scientific Inc, USA). Black carbon (BC) in $PM_{2.5}$ was measured using a

140 seven-wavelength Aethalometer (AE33, Magee Scientific Crop.) (Drinovec et al., 2015). The non-refractory chemical compositions of fine particles (NR-$PM_{2.5}$), including organics (Org), sulfate (SO_4), nitrate (NO_3), ammonium (NH_4), and chloride (Chl), were measured using an online Time-of-Flight Aerosol Chemical Speciation Monitor (ToF-ACSM, Aerodyne Research Inc. U.S.) equipped with a $PM_{2.5}$ aerodynamic lens and a standard vaporizer (Jayne et al., 2000;Drewnick et al., 2005;Cai et al., 2020).

145 Concerning particle number size distributions, particles in the size range of 1 nm - 10 μm were measured using a diethylene glycol scanning mobility particle spectrometer (DEG-SMPS, 1-7.5 nm) (Jiang et al., 2011) and a particle size distribution system (PSD, 3 nm-10 μm) (Liu et al., 2016a;Yan et al., 2021;Deng et al., 2020). Based on this particle distribution information, the condensation sink (CS) (Kulmala et al., 2005) of sulfuric acid was then calculated according to method proposed by Kulmala et al. (2012). Additionally, a neutral cluster and air ion spectrometer (NAIS, model 4-11, Airel, Estonia) was used to detect

150 ions in the size range of 0.7–42 nm (mobility diameter) and particles in the size range of 2.5–42 nm (mobility diameter) (Mirme and Mirme, 2013;Manninen et al., 2016;Zhou et al., 2020).

2.3 Calculation of averaged oxygen and nitrogen numbers of total OOMs

The fraction weighted oxygen and nitrogen numbers of OOMs are calculated based on the following equations:

$$nO(t) = \sum_{i=1}^{n} nO_i \times Fraction_i(t) \qquad (2)$$

$$nN(t) = \sum_{i=1}^{n} nN_i \times Fraction_i(t) \qquad (3)$$

where n is the number of OOM molecules, i is one specific OOM molecule, nO_i (nN_i) is the number of oxygen (nitrogen) in OOM_i, $Fraction_i$ is the number fraction that OOM_i takes, and t is one certain moment. Then, nO and nN could reflect the averaged oxygen and nitrogen number of total OOMs at each moment. Here, we use nO to generally reflect the oxidation state of total OOMs, and the higher of the nO, the more oxidized of total OOMs.

2.4 Division of different periods

In this study, we focus on the four-year variability of air quality in winter Beijing (abbreviated as four-year variability in the following text), as well as the influence of special events, including the Beijing Winter Olympics (Olympics), COVID lockdown (COVID) and Chinese New Year (CNY) during the four years from 2019 to 2022. Thus, the whole winter period from 1st January to 20th February was divided into two separated ones (**Fig. S1** and **Table 1**):

a. The periods of four-year variability. When the four-year variability is investigated, there should be no disturbance from any of the special events, and the chosen days should be from the same periods of different years. Therefore, the period of four-year variability covered days from 1st to 22nd January of each year, lasting for 22 days.

b. The periods of special events. To ensure comparable durations for special events, days ranging from 4th to 20th February were chosen as the special event periods. The days within this date range in 2020 and 2022 are referred to as COVID and Olympics periods, respectively. Since CNY holidays in 2022 interfered with Olympics, only CNY holidays in 2019 and 2021 were used and combined together as the CNY period. Finally, for a better understanding of the special event effect, a Reference period including the non-event days in 2019 and 2021 was chosen as the "base-period".

3. Results and discussion

3.1 Four-year variability of air quality

3.1.1 Meteorological conditions

Meteorological conditions are strongly interlinked with air quality. Therefore, we first focus on the four-year changes of meteorological parameters. The periods covered the days from 1st to 22nd January of each year. As shown in **Fig. 1**, the local wind distributions in 2019 and 2020 were quite similar, following the typical diurnal wind pattern in Beijing induced by the mountain-valley breeze. From midnight to noon, the wind mainly blew from the northwest, and the wind speed (WS) was quite low (median ~ 0.5 m s^{-1}). From afternoon, however, the wind direction turned to a southerly wind. In 2021, the wind was mostly from the west and northwest without a clear diurnal variation. In 2022, the wind blew mostly from the southeast from midnight

to noon, but came from northeast from afternoon to midnight. Usually, the air masses coming from the south or east possess higher temperatures and bring more water vapor as well as pollutants, whereas air masses coming from the north or west are typically colder with a lower RH and lower pollutant concentrations (Wang et al., 2013;Zhong et al., 2018). The year of 2021 witnessed the lowest median temperature (-2.0 °C, **Fig. 2a**) and lower RH (24 %, **Fig. 2b**) compared with other three years, which might be partly due to the wind coming mainly from west and northwest throughout the day. Meanwhile, the overall wind speed in 2021 was also the highest (median 0.75 m s^{-1}, **Fig. 1** and **Fig. 2d**). As the typical diurnal pattern of wind direction in Beijing is induced by the mountain-valley breeze which is usually occurring only during rather stagnant synoptic conditions, the lack of diurnal pattern of wind direction and the higher wind speeds in 2021 suggest that the synoptic meteorological conditions might have been stronger during this period in 2021 than in the other years. Similarly, BLH in 2021 was also the highest throughout the day (**Fig. 2e, f**). During the other three years, the overall values of the temperature, wind speed and BLH were comparable to each other, whereas the RH was higher in 2020 and 2022, which could be partly attribute to more southern and eastern winds in these two years. In addition, differences in cloud conditions could have a minor effect on UVB together with varying pollution conditions. Higher values of RH may facilitate the hygroscopic growth of aerosol particles (Hodas et al., 2014;Cheng et al., 2016) and change the particle phase state, thereby likely promoting the secondary aerosol formation via heterogeneous reactions (Hung et al., 2016;Chao et al., 2020;Shiraiwa et al., 2017;Sun et al., 2018). Furthermore, precipitation can increase the wet deposition of almost all gaseous and particulate species, influencing their concentrations in the atmosphere. However, since there was no reliable measurement of precipitation at our site, detailed conclusions on this matter cannot be drawn. It should be mentioned that the intensity of snow precipitation in winter Beijing is generally small, except during special case(s), so that the overall effects of precipitation in winter Beijing is not as larger as that in summer Beijing or in other humid areas.

3.1.2 Trace gases

The four-year variations of CO and NO$_2$ were generally opposite to that of BLH, which decreased from 2019 to 2021 and rebounded in 2022, resulting in the lowest concentrations in 2021 (**Fig. 3 a, c**, median values are 308 and 12.8 ppb for CO and NO$_2$, respectively). Although the relative changes of them were larger than BLH, the variations of them should be partially attributed to the change in BLH, or the change in atmospheric diffusion capacity. Besides, the winds in 2021 came less frequently from polluted sectors, which might also play a role. For NO, it decreased from 2019 (median 10.8 ppb) to 2021 (median 5.5 ppb), and was around the same level in 2021 and 2022 (**Fig. 3 b**). NO is mainly a primary emission, and in urban Beijing, it mainly comes from vehicle emissions. Although the BLH was lower and the wind was more polluted in 2022 than in 2021, NO levels between these two years are nearly the same, suggesting that traffic emissions might have reduced in 2022. Despite the influence of different wind direction and speed, SO$_2$ concentration monotonically decreased from 2019 (median 3.06 ppb) to 2022 (median 0.68 ppb). Besides, this trend is quite different from that of BLH, indicating that the drop of SO$_2$ is not caused by the variations of meteorology conditions, but by the decline in SO$_2$ emissions. Our result is in line with the long-term variation of SO$_2$ in China, where SO$_2$ decreased from 24.8 ppb in 2013 to 8.0 ppb in 2017 for the Beijing-Tianjin-Hebei area after the clean air action in 2013 (Wang et al., 2020d). The four-year variation of O$_3$ was generally opposite to CO and NO$_2$, and its concentration was the highest in 2021 (15.4 ppb, **Fig. 3d**). This highest O$_3$ could be partly associated with the weakened titration effect of NO. Meanwhile, the level of O$_3$ decreased with the increase of PM$_{2.5}$ (**Fig. S6**), suggesting that O$_3$ formation might be suppressed during haze episodes within the studied period.

3.1.3 Condensable vapors

220   SA is a key contributor to the formation and initial growth of aerosol particles (Sipilä et al., 2010;Paasonen et al., 2010;Kirkby et al., 2011;Yao et al., 2018;Yan et al., 2021), and OOMs are the main drivers of the particle growth and formation of secondary organic aerosol (SOA) (Ehn et al., 2014;Nie et al., 2022). Therefore, for further investigation of number size distributions and mass concentrations of particles, the four-year changes of SA and OOMs were first analyzed. As shown in **Fig. 4**, the concentrations of sulfuric acid monomer (SA1, $4.5 - 9.6 \times 10^5$ cm^{-3}, **Fig. 4a**) and dimer (SA2, $3.1 \times 10^3 - 2.8 \times 10^4$ cm^{-3}, **Fig.**

225   **4b**) generally decreased from 2019 to 2022. This decreasing trend is similar to that of SO$_2$, and therefore, the decline of SA1 and SA2 was probably mainly caused by the drop of the precursor SO$_2$. Additionally, SA2 in 2021 was higher than 2020 and 2022. **Fig. 5** shows that although the data points in 2021 stand out in the SA2 vs. SA1 plot, they lie together with the data points of the other three years in the SA2 vs. $[SA1]^2/CS$ plot. Thus, the elevated SA2 in 2021 was likely caused by the low-level CS (**Fig. S4**).

230   The four-year variation of the total OOM concentration was generally opposite to that of the BLH. Specifically, the median OOM concentration in 2019 (2.4×10^7 cm^{-3}) was ~ 8.6 times of that in 2021 (2.8×10^6 cm^{-3}) (**Fig. 4c**), while median and peak BLH values in 2019 (360 m and ~940 m for median and peak respectively) were only ~$0.7 - 0.8$ times of that in 2021 (497 m and ~1200 m for median and peak respectively) (**Fig. 2e and 2f**). Thus, the reasons behind this drastic yearly change of the OOM concentration cannot be solely attributed to changes in the BLH. Under polluted conditions, regional transportation of lower-volatility OOMs could result in higher concentration of OOMs (Guo et al., 2022). Besides, accumulation of precursor

235   VOCs, and possibly an enhancement of heterogeneous reactions (Riedel et al., 2015), may promote the chemical formation of OOMs. However, due to the lack of VOC measurements and inadequate understanding of heterogeneous reactions, it is hard to conclude which one is the determining factor for the observed OOM concentration changes. Additionally, the total OOM concentrations at same PM$_{2.5}$ levels generally decreased from 2019 to 2022 (**Fig. S7**), which implies that the OOM

240   concentrations have reduced in recent years. In terms of the OOM composition, **Figs. 4d and 4e** show that both oxygen and nitrogen contents of OOMs increased year by year. None of the meteorology parameters showed such a behavior, so changes in the chemical pathways is likely the main cause. The increase in the oxygen content indicates an enhancement of the overall oxidation state of OOMs, and the increase in the nitrogen content is related to an enhancement of the NO$_x$ involvement in OOM formation. Although there are no direct VOC measurements, studies have shown that the VOC levels are continuously

245   decreasing in the region (Yao et al., 2022). Therefore, by assuming that the level of oxidants stays the same, the oxidants to VOCs ratio increases, thus likely leading to more oxidation of each VOC molecule. Besides, long-term observations have shown that the concentration decrease of NO$_x$ is slower than that of VOCs (Yao et al., 2022;Li et al., 2020b). As a result, the NO$_x$ to VOCs ratio should have increased with time, which may partially explain the increased OOM nitrogen content. Furthermore, the oxygen content decreases as PM$_{2.5}$ is increasing. This is not surprising, as OOMs with lower oxygen contents

250   possess higher volatilities, and thus are more easily to be re-evaporated back to the atmosphere and transported along with PM$_{2.5}$. The nitrogen content first increases with an increasing PM$_{2.5}$ levels and then decreases when PM$_{2.5}$ exceeds 150 μg cm^{-3}. Higher PM$_{2.5}$ levels seem to be associated with higher NO$_x$ concentrations (**Fig. S6**), which promotes the formation of organonitrates, leading to a higher nitrogen content. But the reason why the nitrogen content decreases under serve haze remains a puzzle, deserving further studies. In order to evaluate the OOM contribution to SOA formation through condensation, the

255   parameter [ELVOCs + LVOCs] × CS was used as a simple surrogate for OOM condensation flux (**Fig. 4f**). [ELVOCs + LVOCs] × CS was the highest in 2019 and the lowest in 2021, with 2020 and 2022 lying between and being comparable. This suggests

that the SOA formation potential of OOMs was highest in 2021 and lowest in 2021, which is in consistent with the organic aerosol concentration in **Fig. 10**.

3.1.4 Particles and ions

Figure 6 shows the four-year changes of number concentrations of particles in different size ranges. The number concentration of sub-3 nm particles ($N_{1.3-3}$) decreased from 2019 to 2021, but increased slightly from 2021 to 2022. The influencing factors behind this variability are discussed in the following text. Number concentrations in the nucleation mode (3-25 nm, N_{3-25}) and Aitken mode (25-100 nm, N_{25-100}), generally decreased from 2019 to 2022. Especially, N_{3-25} was significantly lower in 2022 than in the other years, which could be attributed to fewer nucleated particles growing into larger sizes when NPF events occurred in 2022 (as shown in **Fig. S2**). In contrast, the OOMs concentration was higher in 2022 than in 2021 (**Fig. 4c**), so reasons for the less efficient grow of the nucleation mode particles in 2022 should be explored further. The accumulation mode particle number concentration ($N_{100-1000}$) was significantly lower in 2021 than in other years, suggesting a suppressed growth of particles from the Aitken mode to larger sizes in measured air masses. This is consistent with the fact that the wind was mainly from northwest in 2021, bringing clean air with low gaseous precursor concentrations. Thus, the overall low $N_{100-1000}$ in 2021 could also be associated with the more frequent clean air episodes with $PM_{2.5} \leq 35$ μg cm^{-3} in 2021 (67%, **Fig. S3a**).

The four-year variation of $N_{1.3-3}$ was contributed by several factors associated with both sources and sinks of these particles. In urban Beijing, as reported in previous studies (Cai et al., 2021;Deng et al., 2021;Deng et al., 2020;Du et al., 2022a), the formation and growth of new particles is influenced by the SA concentration, background aerosol population, amine concentration and ambient temperature, among other things. The SA concentration decreased from 2019 to 2022, and the $PM_{2.5}$ mass concentration, which is strongly associated with the coagulation caused by background aerosols, was the lowest in 2021 (**Fig. 9**). Also, as shown in **Fig. 2**, the ambient temperature was the lowest in 2021, causing favorable conditions for the formation of new particles because small clusters evaporate less efficiently when temperatures are lower. However, with such favorable conditions, the $N_{1.3-3}$ was still the lowest in 2021. The intensities of NPF events were lower in 2021 than 2022, while the NPF event frequency was higher in 2021. A possible reason for this observation is amines, the concentrations of which could have been reduced in 2021 due to limited traffic emissions (indicated by NO_x). However, the influence of this factor is uncertain without simultaneous measurements. The opposite four-year change of BLH can also partly explain that of $N_{1.3-3}$.

Unlike the number concentration of sub-3 nm particles, the ion concentrations in both 0.8-2 ($N_{0.8-2,\ ions}$) and 2-4 nm ($N_{2-4,\ ions}$) size ranges were higher in 2021 than in the other years (**Fig. 7**), possibly due to variations in ion source strengths. The ion concentration was higher in the size range of 0.8-2 nm than in the size range of 2-4 nm, which is consistent with previous studies (Kulmala et al., 2013). **Figure S8** shows the levels of $N_{1.3-3}$ and $N_{0.8-2,\ ions}$ under different pollution level among those four years. We found that $N_{1.3-3}$ decreased with the increasing $PM_{2.5}$ levels, while sub-2 nm ions showed relatively constant concentrations under different pollution levels. Both sub-3 nm particles and sub-2 nm ions are easily to be scavenged by larger particles, and ions are more vulnerable considering their higher diffusivity. The relatively constant concentrations of sub-2 nm ions under different pollution levels might result from that the ion source strengths increased as $PM_{2.5}$ concentration increased, which needs further exploration.

Figure 8 shows that there was a positive and relatively strong association between the concentrations of 2-3 nm particles and the concentrations of SA1 and SA2 in every year, probably because the formation and growth of nucleated particles is strongly

dependent on SA. A weak positive association was also observed between the 2-4 nm ion concentration and SA1 and SA2 concentration. Since 2-4 nm ions originate from collisions between small ions and particles, their concentration is expected to be correlated with SA2, especially as the concentrations of 2-3 nm particles were strongly correlated with concentrations of SA2.

3.1.5 PM$_{2.5}$ and its compositions

The PM$_{2.5}$ mass concentration generally decreased from 2019 to 2021, while rebounding in 2022 to reach a similar level as in 2020 (**Fig. 9**). In 2019, although the median value was similar to those in 2020 and 2022, the average PM$_{2.5}$ mass concentration was higher than in 2020 and 2022. This is because there were more severe haze events in 2019 (PM$_{2.5}$ > 150 μg cm^{-3}, 7%, **Fig. S3a**), which increased the average PM$_{2.5}$ mass concentration considerably. The lowest PM$_{2.5}$ mass concentration coincides with the highest BLH in 2021 (**Fig. 2e, f**). In addition, winds were mainly from northwest in 2021, bringing clean air masses with low PM loadings, and hence the frequency of PM$_{2.5}$ ≤ 35 μg cm^{-3} was the highest in 2021 (67%, **Fig. S3**). These results indicate the important influence of meteorological conditions on air quality. PM$_{2.5}$ concentrations are also driven by primary emissions and secondary production, discussed in more detail below.

The mass concentrations of Chl, BC and Org showed similar four-year variations as the PM$_{2.5}$ mass concentration, with a decrease from 2019 to 2021 and then an increase in 2022 (**Fig. 10**). Related mainly to primary sources, the mass concentrations of Chl and BC had similar four-year variations as CO, a tracer for combustion sources. The mass concentration of Org had a similar four-year variation as Chl and BC, which is because primary emissions like combustions partly contribute to the Org in the particle phase. Another important contributor to Org is secondary formation processes. Previous studies suggest that OOMs, which also decreased from 2019 to 2021 and then increased in 2022, can contribute a substantial fraction to secondary organic aerosol mass concentrations (Nie et al., 2022), Therefore, the four-year variation of Org can be attributed to both primary emissions and secondary production processes.

However, unlike Chl, BC and Org, sulfate showed the lowest concentration in 2022. The generally decreasing trend of the sulfate mass concentration is consistent with the decreasing trend of the SO$_2$ concentration from 2019 to 2022, reflecting the significant reduction of SO$_2$ emissions that China has made during the recent years, especially in winter.

Nitrate and ammonium had their lowest concentrations in 2021 with an increase in 2022 but, unlike Chl, BC and Org, they had higher concentrations in 2020 than in 2019. The similar four-year changes of nitrate and ammonium is mainly because ammonium tends to be associated with nitrate and sulfate in the particle phase, and the contribution of nitrate becomes dominant due to the significant reduction of SO$_2$ emissions. With lower NO$_x$ in 2020 than 2019 (**Fig. 3b, c**), the higher NO$_3$ concentrations in 2020 than those in 2019 suggest that more nitrogen oxides were transformed into particulate nitrate. **Figure S12** shows that at almost all PM$_{2.5}$ levels, the mass concentration of nitrate in 2020 was higher than that in 2019, while NO$_2$ and NO concentrations were generally lower in 2020. One possible reason for this is the much higher RH in 2020, leading to more aerosol liquid water content, which promotes the uptake of HNO$_3$ and the hydrolysis of N$_2$O$_5$ (Wang et al., 2020c).

Despite some four-year variations of the mass fractions of the different aerosol component, Org always contributed the largest fraction to the mass concentration of PM$_{2.5}$ in every year, followed by nitrate (**Fig. 11a**). The nitrate fraction generally increased from 20% in 2019 to 28% in 2022, suggesting the more and more important role of nitrate formation. The important role of the

organics and nitrate in the PM$_{2.5}$ composition has also been found in previous studies in Beijing (Xu et al., 2019;Sun et al., 2020;Hu et al., 2021).

Figure 11b shows that when the PM$_{2.5}$ mass concentration increased from smaller than 35 μg m^{-3} to larger than 150 μg m^{-3}, the mass fraction of secondary inorganic aerosol (SIA), including nitrate, sulfate and ammonium, increased while the mass fraction of organics decreased in every year. This phenomenon was mainly driven by the increase of the nitrate fraction. Especially in 2021 and 2022 when the PM$_{2.5}$ mass concentration was between 35 and 150 μg m^{-3}, the mass fraction of nitrate was the largest among the different components. Our results indicate the important role of nitrate to haze formation and the urgent need for significantly reductions in NO$_x$ emissions in order to improve the air quality in Beijing.

A number of studies have investigated the yearly changes of chemical compositions of particulate matter in Beijing in recent years (Wang et al., 2019;Xu et al., 2019;Zhou et al., 2019;Zhang et al., 2020;Hu et al., 2021). Due to the implementation of air quality regulations, most of the compounds in particulate matter have decreased significantly. For example, chloride of PM$_1$ decreased by 65-89% from 2011-2012 to 2017-2018 in urban Beijing using an ACSM (Zhou et al., 2019). In this study, organics concentration also decreased by 37-70%. However, the nitrate concentration did not decrease but even increased. The nitrate concentration was also found to increase by ~4% during winter time from 2007 to 2017 in a previous study (Zhang et al., 2020). Additionally, many studies found that nitrate gradually becomes the major contributor to the chemical composition of particulate matter, overweighing organics, especially during severe haze periods (Xu et al., 2019;Hu et al., 2021). These results are consistent with ours, indicating the importance of reducing NO$_x$ concentration in Beijing.

3.2 The influence of different special events on air quality

3.2.1 Meteorological conditions

There are three notable meteorological characteristics for the special event periods. First, the wind direction distribution during Reference, CNY and COVID periods were generally similar and followed the typical diurnal wind pattern in Beijing (**Fig. 12a, b, c**). Specifically, from midnight to noon, winds mostly blew from northwest and sometimes also from northeast, while from afternoon to early night, the wind direction turned to the south or southeast. During Olympics, however, the wind pattern was not as strong as in the other events (**Fig. 12d**). From midnight to noon, the dominant wind direction was the southwest, instead of northwest as during the other events. While from afternoon to midnight, there was no prevailing wind direction. This feature could have affected the air quality positively during the Olympics as there were less frequent southerly winds which are typically associated with more polluted air masses. Second, the temperatures during Olympics (median -0.6 ℃) and CNY (median -0.5 ℃) were lower than during Reference (median 2.5 ℃) and COVID (median 2.6 ℃) periods (**Fig. 13a**). The temperature variation may cause changes in the rate of gas- and particle-phase reactions as well as in the volatility of oxygenated organic molecules, and thereby may have slight influence on the air quality. Third, the RH during the COVID period (median 52 %) was higher than during the other three periods (median 24 – 27 %) (**Fig. 13b**). And this high RH may change the phase state of particles and increase the secondary aerosol formation through heterogeneous reactions. Meanwhile, the wind speeds (**Fig. 12** and **Fig. 13d**) and BLH levels (**Fig. 13e, f**) during the four periods were comparable to each other, so that the vertical mixing of air masses was likely relatively similar among different periods.

3.2.2 Trace gases

Since the restrictions during the COVID, Olympics and CNY periods aim at different sections of social life and production activities, trace gases may have different responses to different periods. During Olympics, the southerly wind was not that frequent so that this period was the least influenced by polluted air masses. Consequently, CO, NO, NO_2 and SO_2 were the lowest, and O_3 was the highest during Olympics compared with other three periods. During COVID, however, the southerly wind appeared with the highest frequency, leading to the most severe pollution transportation. Thus, the CO concentration was the highest (849 ppb). It can also be found that, despite the most polluted air masses during COVID, the concentrations of NO, NO_2 and SO_2 were lower than the Reference period, suggesting that the restrictions on NO, NO_2 and SO_2 during that period were quite efficient. Besides, compared with NO_2, the restriction on NO and SO_2 were much more obvious. NO_2 has large sources from secondary formation and is able to transport over long distances (Zhu et al., 2021;Tan et al., 2022), hence, the transportation of NO_2 likely partly compensates the effect of the NO_2 emission control. Under the synergistic influences of pollution transport and COVID control measures, the O_3 concentration was only slightly higher during COVID than during the Reference period. As mentioned before, during CNY, the wind direction had a pattern similar to that during the Reference period, and the wind speed as well as BLH were only slightly higher than those during the Reference period. Therefore, meteorological conditions were similar during these two periods. Consequently, CO was only a bit lower during CNY than during the Reference period. For NO and NO_2, however, their concentrations were much lower during CNY than during the Reference period. This is likely due to the reduction of NO_x emissions from vehicles, as a large fraction of people went hometown from Beijing. Lower NO_x levels also led to higher O_3 levels. The SO_2 concentration was only slightly lower during CNY than during the Reference period. During the winter heating-period in urban Beijing, SO_2 should mainly come from the combustion of fossil fuel (Xu et al., 2016;Meng et al., 2016), so that the reduced traffic emissions had minor influences on SO_2 concentrations. Besides, from New Year's Eve to the next following days, SO_2 can also be emitted from fireworks (Foreback et al., 2022).

We then investigated these gases under different PM levels. When $PM_{2.5}$ exceeded 35 μg m^{-3}, SO_2 during COVID was much lower than during other three periods (**Fig. S10**), and this feature was associated with higher RH (**Fig. S9**) and higher particulate sulfate concentrations (**Fig. S13**). Therefore, the conversion of gaseous SO_2 to particulate sulfate was likely enhanced during COVID when $PM_{2.5}$ was larger than 35 μg m^{-3}, leading to the low concentration of gaseous SO_2. Additionally, O_3 and $PM_{2.5}$ showed a non-linear relationship, O_3 concentration first decreased and then increased with increasing $PM_{2.5}$, for the period from 4th to 20th February (**Fig. S10**), which is consistent with previous studies (Wang et al., 2020d;Zhao et al., 2020). As the level of O_3 is affected by many factors, such as meteorological conditions, regional transport (Lin et al., 2019;Zhao et al., 2021;Liu et al., 2019;Ge et al., 2012), photochemical processes associated with solar radiation, NO_x and VOCs (Tan et al., 2018;Li et al., 2020a), further analysis is highly needed for digging out the reasons behind such behavior of O_3.

In summary, in urban Beijing, concentrations of gaseous pollutants are controlled by their emission sources and the meteorological conditions. Thus, during Olympics, favored by the clean air mass, CO, NO, NO_2 and SO_2 were dramatically reduced. During COVID, under the influence of extremely polluted air masses, the strict restrictions on people's movement which affects traffic emissions, and probably other production activities, CO concentration increased a lot, while NO and SO_2 concentrations reduced, and NO_2 reduced slightly. During CNY, under the influence of unfavorable meteorological conditions, reduced traffic emission and some probably other production activities, CO and SO_2 concentrations didn't decrease, while NO_x reduced.

3.2.3 Condensable vapors

The responses of SA and OOMs to the three restriction periods were quite different. For SA, the concentrations of SA1 and SA2 were the lowest during COVID (median value are 4.2×10^5 cm^{-3} and 5.7×10^3 cm^{-3} for SA1 and SA2, respectively) and were comparable in the other three periods (median values are $6.0 – 8.7 \times 10^5$ cm^{-3} and $1.5 – 1.9 \times 10^4$ cm^{-3} for SA1 and SA2, respectively) (**Fig. 15a, b**). Since SA is mainly produced from SO$_2$ oxidation by OH radicals (Finlayson-Pitts and Pitts Jr., 2000) and is primarily scavenged by condensation onto particles (Dada et al., 2020;Guo et al., 2021;Yang et al., 2021), the lowest concentration during COVID could be attributed to the highest condensation sink (**Fig. S4b**) accompanied by the low SO$_2$ concentration (**Fig. 14e**). Despite the lowest SO$_2$ concentrations during Olympics, SA1 was not low (**Fig. 15a**) and SA2 was even the highest (**Fig. 15b**). This was probably caused by the synergistic effects of decreased condensation sink (**Fig. S4b**) and increased atmospheric oxidation capacity during Olympics (which could be partially indicated by the highest O$_3$, **Fig. 14d**). Meanwhile, compared with COVID and Reference periods, the ratios of SA2/SA1 during Olympics and CNY were higher, suggesting that the cluster formation efficiency of sulfuric acid was enhanced during those two periods.

The concentration of the total OOMs (median values are $1.5 – 2.8 \times 10^7$ cm^{-3}, **Fig. 15d**) was the highest during COVID. Compared with SA, the production and loss processes of OOMs are much more complex: they can be generated from the oxidation of VOCs (volatile organic compounds) and OVOCs (oxygenated volatile organic compounds), or be evaporated from the particle phase (Kohli and Davies, 2021;Yli-Juuti et al., 2017;Wilson et al., 2015). When it comes to the loss processes, OOMs can be consumed by further oxidation processes, or through absorption onto particle surfaces via pure condensation or reactive uptake. Among all these factors, precursor VOCs and OVOCs could have great impacts. Since such precursors tend to come along with pollution (Yao et al., 2021;Niu et al., 2022), OOM concentration also showed a strong association with the pollution level (**Fig. S11**). This is probably why the OOM concentration was the highest during COVID when severe haze (PM$_{2.5}$ > 75 μg m^{-3}) was most frequent, and the lowest during Olympics when there was almost no severe haze (**Fig. 3b**). For OOMs themselves, **Fig. 15** and **Fig. S11** together show that under the same PM$_{2.5}$ level, both the averaged oxygen and nitrogen numbers during Olympics were the highest, which implies that not only the oxidation state of OOMs was enhanced, but also the involvement of NO$_x$ was more effective during Olympics.

3.2.4 Particles and ions

As shown in **Fig. 16**, $N_{1.3-3}$ was almost at the same level during the Reference, COVID, Olympics, and CNY periods. N_{3-25} was lower during CNY period and N_{25-100} were slightly lower during Olympics than during the other periods. However, $N_{100-1000}$ was significantly lower during Olympics compared with the other periods.

The small variability of $N_{1.3-3}$ between the different periods indicate that the special events may have only little effect on the formation of sub-3 nm particles, i.e., new particle formation processes, consistent with a previous study (Yan et al., 2022). However, for the accumulation particles, the significantly lower number concentrations during Olympics indicates a great impact of the reduction of anthropogenic emissions on large particles during this period. Also, the frequent wind direction from the north indicates the transport of clean air mass during Olympics.

Ion concentrations in the different size ranges were significantly higher during Olympics compared with the other periods (**Fig. 17**). During COVID, the ion concentrations were the lowest. Such differences between the different periods basically follow the four-year changes of ion concentrations. As discussed in Sect. 3.1.5, the ion concentrations were higher in 2022 compared

with the other years, which is consistent with the higher ion concentrations during Olympics in 2022 than during the COVID, CNY and Reference periods.

3.2.5 PM$_{2.5}$ and its compositions

The median mass concentration of PM$_{2.5}$ was the lowest during Olympics and the highest during COVID, as compared with the other periods (**Fig. 18**). During the CNY period, the median mass concentration of PM$_{2.5}$ was the second highest. The differences in the PM$_{2.5}$ mass concentration between the different periods were not due to different values of the BLH, since the BLH was similar between the COVID and Olympics periods and the highest during the CNY period (**Fig. 13e**).

Favorable meteorological conditions for transport of clean air mass during Olympics is one of the main reasons leading to the lowest PM$_{2.5}$ mass concentration. In contrast, unfavorable meteorological conditions during the COVID and CNY periods worsened air quality during these two periods. As shown in **Fig. 12**, the wind cycle was obviously different during Olympics than during the other periods. In urban Beijing surrounded by mountains to its west, north and northeast, there is a typical wind cycle with winds tending to come from north or northwest in the morning and from south or southeast in the evening. Such a cycle was obvious during the CNY and COVID periods, allowing the transport of polluted air masses to urban Beijing from the south or southeast, thereby leading to severe haze events.

Another reason for the much lower mass concentrations of PM$_{2.5}$ during Olympics compared with the Reference period were the restriction measures on reducing anthropogenic emissions during this time period. Consistently, there were much lower concentrations of primary particles, i.e., BC and Chl, during Olympics than during the Reference period (**Fig. 19**). Although strict restrictions were also performed during COVID, BC and Chl concentrations were slightly higher than during the Reference period. This should not be interpreted as that emission control was not effective during COVID. In fact, BC during COVID was lower than during the Reference at the same PM$_{2.5}$ levels (**Fig. 13f**). The higher average BC concentration during COVID was associated with the higher frequency of haze episodes during COVID. During CNY, the relatively high primary aerosol concentrations seem to be associated with fireworks.

Secondary aerosol formation is important to understanding PM$_{2.5}$ levels as this process is often the main contributor to the particle mass concentration. The much higher fraction of SIA compared to the other components during COVID (**Fig. 20a**) indicates the enhancement of atmospheric oxidation capacity, which might explain the more severe haze events during this period compared with the other periods. As shown in **Fig. 20b,** the mass fraction of SIA was much higher during COVID, and when the PM$_{2.5}$ mass concentration was higher than 35 μg m^{-3}, the mass fraction of SIA reached almost 70%. The much higher values of RH during COVID could have promoted heterogeneous reactions to produce higher SIA concentrations (**Fig. 13b**). Besides, nitrate showed higher concentrations and mass fractions when PM$_{2.5}$ increased from 35 μg m^{-3} to larger concentrations during COVID than other periods, although there was a reduction in NO$_x$ emissions due to strict restrictions on vehicles this period. This phenomenon indicates that secondary formation of nitrate was enhanced and thus contributed to the formation of haze during COVID. In the case of sulfate, although the SO$_2$ concentration was low during COVID, the overall mass concentration and mass fraction of sulfate was higher than during the other periods, which might be associated with the much higher values of RH during COVID. With higher mass concentrations and fractions of nitrate and sulfate, the ammonium was correspondingly higher during COVID than during the other periods.

4. Summary and conclusions

This study investigated the air quality in megacity Beijing during wintertime, with an emphasis on the four-year changes and the influences of special events (COVID, Olympics and CNY). Numerous variables, including meteorological parameters, concentrations of trace gases, gaseous sulfuric acid and oxygenated organic molecules, number concentrations of atmospheric particles and ions, as well as $PM_{2.5}$ and its composition, were systematically analyzed. The comprehensive datasets span the dates from 1st January to 20th February in the years from 2019 to 2022.

In the first part, the four-year changes of atmospheric parameters were explored, using the datasets from 1st to 22nd January. Generally, the meteorological conditions for 2019 and 2020 were similar, where temperature, wind speed and BLH are comparable, and the wind mainly blew from the northwest from night to noon and turned to the south from the afternoon. In 2022, the wind mostly blew from the southeast from midnight to noon and turned to the northeast from afternoon. The wind speed in this year was a little higher than 2019 and 2020, and the temperature and BLH were slightly lower than 2019 and 2020. In 2021, the wind was mostly from the west or northwest. Thus, the air masses in this year were much cleaner than other three years due to the least influence of polluted south air masses. This clean condition in 2021 was also associated with the highest wind speed and the maximum BLH, leading to the strongest atmospheric diffusion capacity. Besides, RH showed an increasing pattern from 2019 to 2022, which may facilitate the formation of secondary aerosols through heterogeneous reactions (Sun et al., 2018).

For conventional gaseous and particulate pollutants, the four-year changes of CO, NO_2, total $PM_{2.5}$, organic aerosol, chloride and black carbon were generally opposite to that of BLH that they decreased from 2019 to 2021 and increased in 2022. The atmospheric conditions of 2021 were also the cleanest. Thus, the atmospheric diffusion capacity and the overall cleanness of the air masses may control the variations of the above pollutants. Unlike them, SO_2 monotonically decreased from 2019 (3.06 ppb) to 2022 (0.68 ppb) regardless of the changes in meteorological conditions, suggesting that SO_2 emissions and sources decreased year-by-year. Due to the decline of SO_2, particulate sulfate also decreased from 2019 (2.2 μg m^{-3}) to 2022 (1.1 μg m^{-3}). NO in 2022 was around the same as 2021 despite more polluted conditions, indicating that the traffic emission in 2022 might have reduced. For O_3, it showed an opposite variation with NO_2 that it increased from 2019 (6.3 ppb) to 2021 (15.4 ppb) and dropped in 2022 (8.1 ppb). For nitrate, its contribution to $PM_{2.5}$ increased from 20 % in 2019 to 28 % in 2022. Moreover, its contribution to $PM_{2.5}$ was more pronounced during polluted conditions (PM > 35 μg m^{-3}), indicating the important role of nitrate to haze formation and the urgent need for significantly reductions in NO_x emissions.

For unconventional parameters, owing to the reduction of SO_2, the concentrations of gaseous sulfuric acid monomer and dimer generally decreased from 2019 (9.6×10^5 cm^{-3} and 2.8×10^4 cm^{-3} for sulfuric acid monomer and dimer respectively) to 2022 (4.5×10^5 cm^{-3} and 3.1×10^3 cm^{-3} for sulfuric acid monomer and dimer respectively). For total OOMs, however, its concentration decreased from 2019 to 2021 and increased in 2022. This variation was generally opposite to BLH but with larger extent, suggesting that OOM concentration was controlled both by meteorological conditions as well as local chemical production. Meanwhile, both oxygen and nitrogen contents of gas-phase OOMs increased year by year, implying that not only the oxidation state of those compounds was increased, but also NO_x was involved more efficiently in their formation processes. For particles, it was found that with higher SA concentrations and NPF frequencies in 2021 than in 2022, and with the lowest concentrations of background aerosols and the lowest ambient temperatures in 2021, $N_{1.3-3}$ was still the lowest in 2021. This is out of the scope of conventional understanding and further studies are needed to explore the reasons behind this phenomenon.

In the second part, the influences of special events, including COVID lockdown, Beijing Winter Olympics and Chinese New Year, were investigated, using the datasets from 4th to 20th February. The wind direction distribution during the Reference, COVID and CNY periods were similar that the wind mostly blew from northwest or northeast from midnight to noon and turned to the south or southeast from the afternoon. During the Olympics, however, the dominant wind was from the southwest from midnight to noon, while there was no prevailing wind from the afternoon. Thus, the air masses during Olympics were the cleanest due to less frequent southerly wind. Besides, there was not too much different in wind speed and BLH for four periods. One thing needs to be mentioned is that the RH during COVID was much higher than other three periods, which should promote the growth of secondary aerosols.

During Olympics, favored by the clean conditions, most trace gases (CO, NO, NO_2 and SO_2) and particulate matters (total $PM_{2.5}$, organic aerosol, nitrate, ammonium, chloride and black carbon) were dramatically reduced compared with Reference period. During COVID, influenced by the extremely polluted conditions, CO and all particulate matters (total $PM_{2.5}$, organic aerosol, sulfate, nitrate, ammonium, chloride and black carbon) increased a lot. Despite the serve haze, NO and SO_2 reduced, and NO_2 reduced slightly, suggesting that the restriction on traffic emission and probably other production activities were effective in reducing NO_x and SO_2. Besides, the high RH during COVID likely facilitated the gas-to-particle conversion of sulfur- and nitrogen-containing compounds, resulting in particularly high concentrations of sulfate (8.5 μg m^{-3}), nitrate (16.2 μg m^{-3}) and ammonium (8.6 μg m^{-3}). During CNY, affected by unfavorable meteorological conditions, reduced traffic emission and probably other production activities, CO, SO_2, total $PM_{2.5}$, nitrate and black carbon were comparable with the Reference period, while NO_x reduced, organic aerosol, ammonium and chloride increased, and sulfate increased to a large extent. During that period, O_3 had a non-linear relationship with $PM_{2.5}$ that its concentration first decreased and then increased with increasing $PM_{2.5}$, which is different from the period of 1st – 22nd January. This suggests that the synergetic control strategy of $PM_{2.5}$ and O_3 should consider the effect of seasonality.

SA and OOMs are the secondary products so that their variations were complex and were not directly linked to the changes of meteorology or restriction. The level of SA1 was mainly influenced by CS, SO_2 and UVB (Petäjä et al., 2009;Yang et al., 2021). Compared with Reference period, SA1 was comparable during Olympics, lower during CNY and much lower during COVID. The concentration of SA2 was mainly controlled by SA1 and CS. Compared with Reference period, SA2 during Olympics and CNY were comparable, while much lower during COVID. As COVID was the most polluted, the above results suggest that the formation of SA was suppressed under polluted condition. For total OOMs, however, it had the lowest concentration in Olympics while the highest concentration in COVID, indicating that the level of total OOMs was higher under polluted conditions. Meanwhile, the oxygen content was the highest during Olympics while the lowest during COVID, which implies the oxidation state of OOMs likely decreased with increasing pollution level. For atmospheric particles, $N_{1.3-3}$ was almost the same during Reference, COVID, Olympics and CNY, indicating that the special events may only have little impacts on new particle formation processes. However, $N_{100-1000}$ was significantly lower during Olympics than other periods, suggesting the significant reduction of anthropogenic emissions during this period.

These results provide useful information on how the air quality in urban Beijing has changed in recent for years, and how the air quality was affected by meteorological conditions as well as different emission reduction scenarios. All of these will help in planning more targeted and sustainable long-term pollution control plans.

545   **Data availability:** Datasets for this paper can be accessed at https://doi.org/10.5281/zenodo.7100748 (Guo et al., 2022).

Author contributions: Y.G, C.D, T.K., W.D. and M.K. designed the research; Y.G., C.D., F.Z., Y.L., J.W., C.H., J.Z., Z.W., J.J., Y.Z., T.L., Y.Z., B.S., W.M., Y.L., C.Y., J.J., and M.K. collected the data; Y.G., C.D. and A.O. analyzed data with the help from T.K., W.D., T.N., V.K., M.X., C.Y. and M.K.; Y.G., C.D., T.K. and W.D. wrote the paper with inputs from all co-authors.

550   **Competing interests:** The authors declare no competing interests.

Acknowledgements: We acknowledge the following projects: the National Natural Science Foundation of China (92044301); ACCC Flagship funded by the Academy of Finland grant number 337549; Academy professorship funded by the Academy of Finland (grant no. 302958); Academy of Finland projects no. 1325656, 311932, 316114, 332547, and 325647; "Quantifying carbon sink, CarbonSink+ and their interaction with air quality" INAR project funded by Jane and Aatos Erkko Foundation;

555   European Research Council (ERC) project ATM-GTP Contract No. 742206; "Air pollution cocktail in Gigacity" by The Jenny and Antti Wihuri Foundation. Technical and scientific staff in Beijing, AHL/BUCT laboratory are acknowledged.

References

An, Z., Huang, R. J., Zhang, R., Tie, X., Li, G., Cao, J., Zhou, W., Shi, Z., Han, Y., Gu, Z., and Ji, Y.: Severe haze in northern China: A synergy of anthropogenic emissions and atmospheric processes, Proceedings of the National Academy of Sciences of the United States of America, 116, 8657-8666, 10.1073/pnas.1900125116, 2019.

Bianchi, F., Kurten, T., Riva, M., Mohr, C., Rissanen, M. P., Roldin, P., Berndt, T., Crounse, J. D., Wennberg, P. O., Mentel, T. F., Wildt, J., Junninen, H., Jokinen, T., Kulmala, M., Worsnop, D. R., Thornton, J. A., Donahue, N., Kjaergaard, H. G., and Ehn, M.: Highly Oxygenated Organic Molecules (HOM) from Gas-Phase Autoxidation Involving Peroxy Radicals: A Key Contributor to Atmospheric Aerosol, Chem Rev, 119, 3472-3509, 10.1021/acs.chemrev.8b00395, 2019.

Cai, J., Chu, B., Yao, L., Yan, C., Heikkinen, L. M., Zheng, F., Li, C., Fan, X., Zhang, S., Yang, D., Wang, Y., Kokkonen, T. V., Chan, T., Zhou, Y., Dada, L., Liu, Y., He, H., Paasonen, P., Kujansuu, J. T., Petäjä, T., Mohr, C., Kangasluoma, J., Bianchi, F., Sun, Y., Croteau, P. L., Worsnop, D. R., Kerminen, V.-M., Du, W., Kulmala, M., and Daellenbach, K. R.: Size-segregated particle number and mass concentrations from different emission sources in urban Beijing, Atmospheric Chemistry and Physics, 20, 12721-12740, 10.5194/acp-20-12721-2020, 2020.

Cai, R., Yan, C., Yang, D., Yin, R., Lu, Y., Deng, C., Fu, Y., Ruan, J., Li, X., Kontkanen, J., Zhang, Q., Kangasluoma, J., Ma, Y., Hao, J., Worsnop, D. R., Bianchi, F., Paasonen, P., Kerminen, V.-M., Liu, Y., Wang, L., Zheng, J., Kulmala, M., and Jiang, J.: Sulfuric acid–amine nucleation in urban Beijing, Atmospheric Chemistry and Physics, 21, 2457-2468, 10.5194/acp-21-2457-2021, 2021.

Chao, H.-J., Huang, W.-C., Chen, C.-L., Chou, C. C. K., and Hung, H.-M.: Water Adsorption vs Phase Transition of Aerosols Monitored by a Quartz Crystal Microbalance, ACS Omega, 5, 31858-31866, 10.1021/acsomega.0c04698, 2020.

Chen, C., Sun, Y. L., Xu, W. Q., Du, W., Zhou, L. B., Han, T. T., Wang, Q. Q., Fu, P. Q., Wang, Z. F., Gao, Z. Q., Zhang, Q., and Worsnop, D. R.: Characteristics and sources of submicron aerosols above the urban canopy (260 m) in Beijing, China, during the 2014 APEC summit, Atmospheric Chemistry and Physics, 15, 12879-12895, 10.5194/acp-15-12879-2015, 2015.

Cheng, Y., Engling, G., He, K. B., Duan, F. K., Ma, Y. L., Du, Z. Y., Liu, J. M., Zheng, M., and Weber, R. J.: Biomass burning contribution to Beijing aerosol, Atmospheric Chemistry and Physics, 13, 7765-7781, 10.5194/acp-13-7765-2013, 2013.

Cheng, Y., Zheng, G., Wei, C., Mu, Q., Zheng, B., Wang, Z., Gao, M., Zhang, Q., He, K., Carmichael, G., Pöschl, U., and Su, H.: Reactive nitrogen chemistry in aerosol water as a source of sulfate during haze events in China, Science Advances, 2, e1601530, doi:10.1126/sciadv.1601530, 2016.

Dada, L., Ylivinkka, I., Baalbaki, R., Li, C., Guo, Y., Yan, C., Yao, L., Sarnela, N., Jokinen, T., Daellenbach, K. R., Yin, R., Deng, C., Chu, B., Nieminen, T., Kontkanen, J., Stolzenburg, D., Sipilä, M., Hussein, T., Paasonen, P., Bianchi, F., Salma, I., Weidinger, T., Pikridas, M., Sciare, J., Jiang, J., Liu, Y., Petäjä, T., Kerminen, V. M., and Kulmala, M.: Sources and sinks driving sulphuric acid concentrations in contrasting environments: Implications on proxy calculations, Atmospheric Chemistry and Physics, 20, 11747-11766, 10.5194/acp-20-11747-2020, 2020.

Deng, C., Fu, Y., Dada, L., Yan, C., Cai, R., Yang, D., Zhou, Y., Yin, R., Lu, Y., Li, X., Qiao, X., Fan, X., Nie, W., Kontkanen, J., Kangasluoma, J., Chu, B., Ding, A., Kerminen, V. M., Paasonen, P., Worsnop, D. R., Bianchi, F., Liu, Y., Zheng, J., Wang, L., Kulmala, M., and Jiang, J.: Seasonal Characteristics of New Particle Formation and Growth in Urban Beijing, Environ Sci Technol, 54, 8547-8557, 10.1021/acs.est.0c00808, 2020.

Deng, C., Cai, R., Yan, C., Zheng, J., and Jiang, J.: Formation and growth of sub-3 nm particles in megacities: impact of background aerosols, Faraday Discuss, 226, 348-363, 10.1039/d0fd00083c, 2021.

Drewnick, F., Hings, S. S., DeCarlo, P., Jayne, J. T., Gonin, M., Fuhrer, K., Weimer, S., Jimenez, J. L., Demerjian, K. L., Borrmann, S., and Worsnop, D. R.: A new Time-of-Flight Aerosol Mass Spectrometer (TOF-AMS)—Instrument description and first field deployment, Aerosol Science and Technology, 39, 637-658, 10.1080/02786820500182040, 2005.

Drinovec, L., Močnik, G., Zotter, P., Prévôt, A. S. H., Ruckstuhl, C., Coz, E., Rupakheti, M., Sciare, J., Müller, T., Wiedensohler, A., and Hansen, A. D. A.: The "dual-spot" Aethalometer: an improved measurement of aerosol black carbon with real-time loading compensation, Atmos. Meas. Tech., 8, 1965-1979, 10.5194/amt-8-1965-2015, 2015.

Du, W., Dada, L., Zhao, J., Chen, X., Daellenbach, K. R., Xie, C., Wang, W., He, Y., Cai, J., Yao, L., Zhang, Y., Wang, Q., Xu, W., Wang, Y., Tang, G., Cheng, X., Kokkonen, T. V., Zhou, W., Yan, C., Chu, B., Zha, Q., Hakala, S., Kurppa, M., Järvi, L., Liu, Y., Li, Z., Ge, M., Fu, P., Nie, W., Bianchi, F., Petäjä, T., Paasonen, P., Wang, Z., Worsnop, D. R., Kerminen, V.-M.,

605   Kulmala, M., and Sun, Y.: A 3D study on the amplification of regional haze and particle growth by local emissions, npj Climate and Atmospheric Science, 4, 10.1038/s41612-020-00156-5, 2021.

Du, W., Cai, J., Zheng, F., Yan, C., Zhou, Y., Guo, Y., Chu, B., Yao, L., Heikkinen, L. M., Fan, X., Wang, Y., Cai, R., Hakala, S., Chan, T., Kontkanen, J., Tuovinen, S., Petäjä, T., Kangasluoma, J., Bianchi, F., Paasonen, P., Sun, Y., Kerminen, V.-M., Liu, Y., Daellenbach, K. R., Dada, L., and Kulmala, M.: Influence of Aerosol Chemical Composition on Condensation Sink

610   Efficiency and New Particle Formation in Beijing, Environmental Science & Technology Letters, 9, 375-382, 10.1021/acs.estlett.2c00159, 2022a.

Du, W., Wang, W., Liu, R., Wang, Y., Zhang, Y., Zhao, J., Dada, L., Xie, C., Wang, Q., Xu, W., Zhou, W., Zhang, F., Li, Z., Fu, P., Li, J., Kangasluoma, J., Wang, Z., Ge, M., Kulmala, M., and Sun, Y.: Insights into vertical differences of particle number size distributions in winter in Beijing, China, Sci. Total Environ., 802, 10.1016/j.scitotenv.2021.149695, 2022b.

615   Ehn, M., Thornton, J. A., Kleist, E., Sipilä, M., Junninen, H., Pullinen, I., Springer, M., Rubach, F., Tillmann, R., Lee, B., Lopez-Hilfiker, F., Andres, S., Acir, I.-H., Rissanen, M., Jokinen, T., Schobesberger, S., Kangasluoma, J., Kontkanen, J., Nieminen, T., Kurtén, T., Nielsen, L. B., Jørgensen, S., Kjaergaard, H. G., Canagaratna, M., Maso, M. D., Berndt, T., Petäjä, T., Wahner, A., Kerminen, V.-M., Kulmala, M., Worsnop, D. R., Wildt, J., and Mentel, T. F.: A large source of low-volatility secondary organic aerosol, Nature, 506, 476-479, 10.1038/nature13032, 2014.

620   Finlayson-Pitts, B. J., and Pitts Jr., J. N.: Chemistry of the Upper and Lower Atmosphere: Theory, Experiments, and Applications, Academic Press, San Diego, CA, USA, 298–299 pp., 2000.

Foreback, B., Dada, L., Daellenbach, K. R., Yan, C., Wang, L., Chu, B., Zhou, Y., Kokkonen, T. V., Kurppa, M., Pileci, R. E., Wang, Y., Chan, T., Kangasluoma, J., Zhuohui, L., Guo, Y., Li, C., Baalbaki, R., Kujansuu, J., Fan, X., Feng, Z., Rantala, P., Gani, S., Bianchi, F., Kerminen, V. M., Petäjä, T., Kulmala, M., Liu, Y., and Paasonen, P.: Measurement report: A multi-year

625   study on the impacts of Chinese New Year celebrations on air quality in Beijing, China, Atmos. Chem. Phys., 22, 11089-11104, 10.5194/acp-22-11089-2022, 2022.

Ge, B., Wang, Z., Lin, W., Xu, X., Li, J., Ji, D., and Ma, Z.: Air pollution over the North China Plain and its implication of regional transport: A new sight from the observed evidences, Environmental pollution, 234, 29-38, 10.1016/j.envpol.2017.10.084, 2018.

630   Ge, B. Z., Xu, X. B., Lin, W. L., Li, J., and Wang, Z. F.: Impact of the regional transport of urban Beijing pollutants on downwind areas in summer: ozone production efficiency analysis, Tellus B: Chemical and Physical Meteorology, 64, 17348, 10.3402/tellusb.v64i0.17348, 2012.

Guo, J., Deng, M., Lee, S. S., Wang, F., Li, Z., Zhai, P., Liu, H., Lv, W., Yao, W., and Li, X.: Delaying precipitation and lightning by air pollution over the Pearl River Delta. Part I: Observational analyses, Journal of Geophysical Research:

635   Atmospheres, 121, 6472-6488, 10.1002/2015jd023257, 2016.

Guo, Y., Yan, C., Li, C., Ma, W., Feng, Z., Zhou, Y., Lin, Z., Dada, L., Stolzenburg, D., Yin, R., Kontkanen, J., Daellenbach, K. R., Kangasluoma, J., Yao, L., Chu, B., Wang, Y., Cai, R., Bianchi, F., Liu, Y., and Kulmala, M.: Formation of nighttime sulfuric acid from the ozonolysis of alkenes in Beijing, Atmospheric Chemistry and Physics, 21, 5499-5511, 10.5194/acp-21-5499-2021, 2021.

640   Guo, Y., Yan, C., Liu, Y., Qiao, X., Zheng, F., Zhang, Y., Zhou, Y., Li, C., Fan, X., Lin, Z., Feng, Z., Zhang, Y., Zheng, P., Tian, L., Nie, W., Wang, Z., Huang, D., Daellenbach, K. R., Yao, L., Dada, L., Bianchi, F., Jiang, J., Liu, Y., Kerminen, V. M., and Kulmala, M.: Seasonal Variation of Oxygenated Organic Molecules in Urban Beijing and their Contribution to Secondary Organic Aerosol, Atmos. Chem. Phys. Discuss., 2022, 1-33, 10.5194/acp-2022-181, 2022.

Heinritzi, M., Simon, M., Steiner, G., Wagner, A. C., Kuerten, A., Hansel, A., and Curtius, J.: Characterization of the mass-

645   dependent transmission efficiency of a CIMS, Atmospheric Measurement Techniques, 9, 1449-1460, 10.5194/amt-9-1449-2016, 2016.

Hodas, N., Sullivan, A. P., Skog, K., Keutsch, F. N., Collett, J. L., Decesari, S., Facchini, M. C., Carlton, A. G., Laaksonen, A., and Turpin, B. J.: Aerosol Liquid Water Driven by Anthropogenic Nitrate: Implications for Lifetimes of Water-Soluble Organic Gases and Potential for Secondary Organic Aerosol Formation, Environmental Science & Technology, 48, 11127-

650   11136, 10.1021/es5025096, 2014.

Hu, S., Zhao, G., Tan, T., Li, C., Zong, T., Xu, N., Zhu, W., and Hu, M.: Current challenges of improving visibility due to increasing nitrate fraction in PM2.5 during the haze days in Beijing, China, Environ Pollut, 290, 118032, 10.1016/j.envpol.2021.118032, 2021.

Huang, R. J., Zhang, Y., Bozzetti, C., Ho, K. F., Cao, J. J., Han, Y., Daellenbach, K. R., Slowik, J. G., Platt, S. M., Canonaco, F., Zotter, P., Wolf, R., Pieber, S. M., Bruns, E. A., Crippa, M., Ciarelli, G., Piazzalunga, A., Schwikowski, M., Abbaszade, G., Schnelle-Kreis, J., Zimmermann, R., An, Z., Szidat, S., Baltensperger, U., El Haddad, I., and Prevot, A. S.: High secondary aerosol contribution to particulate pollution during haze events in China, Nature, 514, 218-222, 10.1038/nature13774, 2014.

Hung, H.-M., Hsu, C.-H., Lin, W.-T., and Chen, Y.-Q.: A case study of single hygroscopicity parameter and its link to the functional groups and phase transition for urban aerosols in Taipei City, Atmospheric Environment, 132, 240-248, https://doi.org/10.1016/j.atmosenv.2016.03.008, 2016.

Jayne, J. T., Leard, D. C., Zhang, X., Davidovits, P., Smith, K. A., Kolb, C. E., and Worsnop, D. R.: Development of an aerosol mass spectrometer for size and composition analysis of submicron particles, Aerosol Science and Technology, 33, 49-70, 10.1080/027868200410840, 2000.

Jiang, J., Chen, M., Kuang, C., Attoui, M., and McMurry, P. H.: Electrical Mobility Spectrometer Using a Diethylene Glycol Condensation Particle Counter for Measurement of Aerosol Size Distributions Down to 1 nm, Aerosol Science and Technology, 45, 510-521, 10.1080/02786826.2010.547538, 2011.

Kirkby, J., Curtius, J., Almeida, J., Dunne, E., Duplissy, J., Ehrhart, S., Franchin, A., Gagne, S., Ickes, L., Kuerten, A., Kupc, A., Metzger, A., Riccobono, F., Rondo, L., Schobesberger, S., Tsagkogeorgas, G., Wimmer, D., Amorim, A., Bianchi, F., Breitenlechner, M., David, A., Dommen, J., Downard, A., Ehn, M., Flagan, R. C., Haider, S., Hansel, A., Hauser, D., Jud, W., Junninen, H., Kreissl, F., Kvashin, A., Laaksonen, A., Lehtipalo, K., Lima, J., Lovejoy, E. R., Makhmutov, V., Mathot, S., Mikkila, J., Minginette, P., Mogo, S., Nieminen, T., Onnela, A., Pereira, P., Petaja, T., Schnitzhofer, R., Seinfeld, J. H., Sipila, M., Stozhkov, Y., Stratmann, F., Tome, A., Vanhanen, J., Viisanen, Y., Vrtala, A., Wagner, P. E., Walther, H., Weingartner, E., Wex, H., Winkler, P. M., Carslaw, K. S., Worsnop, D. R., Baltensperger, U., and Kulmala, M.: Role of sulphuric acid, ammonia and galactic cosmic rays in atmospheric aerosol nucleation, Nature, 476, 429-433, 10.1038/nature10343, 2011.

Kohli, R. K., and Davies, J. F.: Measuring the Chemical Evolution of Levitated Particles: A Study on the Evaporation of Multicomponent Organic Aerosol, Analytical Chemistry, 93, 12472-12479, 10.1021/acs.analchem.1c02890, 2021.

Kulmala, M., Petäjä, T., Mönkkönen, P., Koponen, I. K., Dal Maso, M., Aalto, P. P., Lehtinen, K. E. J., and Kerminen, V. M.: On the growth of nucleation mode particles: source rates of condensable vapor in polluted and clean environments, Atmospheric Chemistry and Physics, 5, 409-416, 10.5194/acp-5-409-2005, 2005.

Kulmala, M., Petaja, T., Nieminen, T., Sipila, M., Manninen, H. E., Lehtipalo, K., Dal Maso, M., Aalto, P. P., Junninen, H., Paasonen, P., Riipinen, I., Lehtinen, K. E., Laaksonen, A., and Kerminen, V. M.: Measurement of the nucleation of atmospheric aerosol particles, Nature Protocols, 7, 1651-1667, 10.1038/nprot.2012.091, 2012.

Kulmala, M., Kontkanen, J., Junninen, H., Lehtipalo, K., Manninen, H. E., Nieminen, T., Petäjä, T., Sipilä, M., Schobesberger, S., Rantala, P., Franchin, A., Jokinen, T., Järvinen, E., Äijälä, M., Kangasluoma, J., Hakala, J., Aalto, P. P., Paasonen, P., Mikkilä, J., Vanhanen, J., Aalto, J., Hakola, H., Makkonen, U., Ruuskanen, T., Mauldin, R. L., 3rd, Duplissy, J., Vehkamäki, H., Bäck, J., Kortelainen, A., Riipinen, I., Kurtén, T., Johnston, M. V., Smith, J. N., Ehn, M., Mentel, T. F., Lehtinen, K. E., Laaksonen, A., Kerminen, V. M., and Worsnop, D. R.: Direct observations of atmospheric aerosol nucleation, Science, 339, 943-946, 10.1126/science.1227385, 2013.

Kulmala, M., Dada, L., Dällenbach, K., Yan, C., Stolzenburg, D., Kontkanen, J., Ezhova, E., Hakala, S., Tuovinen, S., Kokkonen, T., Kurppa, M., Cai, R., Zhou, Y., Yin, R., Baalbaki, R., Chan, T., Chu, B., Deng, C., Fu, Y., Ge, M., He, H., Heikkinen, L., Junninen, H., Nei, W., Rusanen, A., Vakkari, V., Wang, Y., Wang, L., yao, l., Zheng, J., Kujansuu, J., Kangasluoma, J., Petäjä, T., Paasonen, P., Järvi, L., Worsnop, D., Ding, A., Liu, Y., Jiang, J., Bianchi, F., Yang, G., Liu, Y., Lu, Y., and Kerminen, V.-M.: Is reducing new particle formation a plausible solution to mitigate particulate air pollution in Beijing and other Chinese megacities?, Faraday Discuss., 10.1039/d0fd00078g, 2020.

Kulmala, M., Cai, R., Stolzenburg, D., Zhou, Y., Dada, L., Guo, Y., Yan, C., Petaja, T., Jiang, J., and Kerminen, V. M.: The contribution of new particle formation and subsequent growth to haze formation, Environ Sci Atmos, 2, 352-361, 10.1039/d1ea00096a, 2022.

Kürten, A., Rondo, L., Ehrhart, S., and Curtius, J.: Calibration of a chemical ionization mass spectrometer for the measurement of gaseous sulfuric acid, The Journal of Physical Chemistry A, 116, 6375-6386, 2012.

700 Le, T., Wang, Y., Liu, L., Yang, J., Yung, Y. L., Li, G., and Seinfeld, J. H.: Unexpected air pollution with marked emission reductions during the COVID-19 outbreak in China, Science, 369, 702-706, 2020.

Li, K., Jacob, D. J., Liao, H., Qiu, Y., Shen, L., Zhai, S., Bates, K. H., Sulprizio, M. P., Song, S., Lu, X., Zhang, Q., Zheng, B., Zhang, Y., Zhang, J., Lee, H. C., and Kuk, S. K.: Ozone pollution in the North China Plain spreading into the late-winter haze season, Proc Natl Acad Sci U S A, 118, 10.1073/pnas.2015797118, 2021.

705 Li, Q., Su, G., Li, C., Liu, P., Zhao, X., Zhang, C., Sun, X., Mu, Y., Wu, M., Wang, Q., and Sun, B.: An investigation into the role of VOCs in SOA and ozone production in Beijing, China, Science of The Total Environment, 720, 137536, https://doi.org/10.1016/j.scitotenv.2020.137536, 2020a.

Li, W., Shao, L., Wang, W., Li, H., Wang, X., Li, Y., Li, W., Jones, T., and Zhang, D.: Air quality improvement in response to intensified control strategies in Beijing during 2013-2019, The Science of the total environment, 744, 140776, 710 10.1016/j.scitotenv.2020.140776, 2020b.

Lin, J. T., and McElroy, M. B.: Detection from space of a reduction in anthropogenic emissions of nitrogen oxides during the Chinese economic downturn, Atmos. Chem. Phys., 11, 8171-8188, 10.5194/acp-11-8171-2011, 2011.

Lin, X., Yuan, Z., Yang, L., Luo, H., and Li, W.: Impact of Extreme Meteorological Events on Ozone in the Pearl River Delta, China, Aerosol and Air Quality Research, 19, 1307-1324, 10.4209/aaqr.2019.01.0027, 2019.

715 Liu, H., Zhang, M., Han, X., Li, J., and Chen, L.: Episode analysis of regional contributions to tropospheric ozone in Beijing using a regional air quality model, Atmospheric Environment, 199, 299-312, https://doi.org/10.1016/j.atmosenv.2018.11.044, 2019.

Liu, J., Jiang, J., Zhang, Q., Deng, J., and Hao, J.: A spectrometer for measuring particle size distributions in the range of 3 nm to 10 μm, Frontiers of Environmental Science & Engineering, 10, 63-72, 10.1007/s11783-014-0754-x, 2016a.

720 Liu, Y., Wu, Z., Wang, Y., Xiao, Y., Gu, F., Zheng, J., Tan, T., Shang, D., Wu, Y., Zeng, L., Hu, M., Bateman, A. P., and Martin, S. T.: Submicrometer Particles Are in the Liquid State during Heavy Haze Episodes in the Urban Atmosphere of Beijing, China, Environmental Science & Technology Letters, 4, 427-432, 10.1021/acs.estlett.7b00352, 2017.

Liu, Y., Yan, C., Feng, Z., Zheng, F., Fan, X., Zhang, Y., Li, C., Zhou, Y., Lin, Z., Guo, Y., Zhang, Y., Ma, L., Zhou, W., Liu, Z., Dada, L., Dällenbach, K., Kontkanen, J., Cai, R., Chan, T., Chu, B., Du, W., Yao, L., Wang, Y., Cai, J., Kangasluoma, J., 725 Kokkonen, T., Kujansuu, J., Rusanen, A., Deng, C., Fu, Y., Yin, R., Li, X., Lu, Y., Liu, Y., Lian, C., Yang, D., Wang, W., Ge, M., Wang, Y., Worsnop, D. R., Junninen, H., He, H., Kerminen, V.-M., Zheng, J., Wang, L., Jiang, J., Petäjä, T., Bianchi, F., and Kulmala, M.: Continuous and comprehensive atmospheric observations in Beijing: A station to understand the complex urban atmospheric environment, Big Earth Data, 4, 295-321, 10.1080/20964471.2020.1798707, 2020.

Liu, Z., Wang, Y., Hu, B., Ji, D., Zhang, J., Wu, F., Wan, X., and Wang, Y.: Source appointment of fine particle number and 730 volume concentration during severe haze pollution in Beijing in January 2013, Environmental science and pollution research international, 23, 6845-6860, 10.1007/s11356-015-5868-6, 2016b.

Lu, X., Zhang, S., Xing, J., Wang, Y., Chen, W., Ding, D., Wu, Y., Wang, S., Duan, L., and Hao, J.: Progress of Air Pollution Control in China and Its Challenges and Opportunities in the Ecological Civilization Era, Engineering, 6, 1423-1431, 10.1016/j.eng.2020.03.014, 2020.

735 Ma, Q., Wu, Y., Zhang, D., Wang, X., Xia, Y., Liu, X., Tian, P., Han, Z., Xia, X., Wang, Y., and Zhang, R.: Roles of regional transport and heterogeneous reactions in the PM2.5 increase during winter haze episodes in Beijing, Sci. Total Environ., 599-600, 246-253, 10.1016/j.scitotenv.2017.04.193, 2017.

Manninen, H. E., Mirme, S., Mirme, A., Petäjä, T., and Kulmala, M.: How to reliably detect molecular clusters and nucleation mode particles with Neutral cluster and Air Ion Spectrometer (NAIS), Atmos. Meas. Tech., 9, 3577-3605, 10.5194/amt-9-740 3577-2016, 2016.

Meng, K., Cheng, X., Xu, X., Qu, X., Ma, C., Zhao, Y., Li, Y., Yang, Y., Zhang, W., and Ding, G.: Spatial-temporal variations of pollutant emission sources inversed by adaptive nudging scheme over Beijing-Tianjin-Hebei region based on the CMAQ model, Journal of Environmental Sciences, 37, 52-60, 0.13671/j.hjkxxb.2016.0240, 2016.

Mirme, S., and Mirme, A.: The mathematical principles and design of the NAIS – a spectrometer for the measurement of cluster 745 ion and nanometer aerosol size distributions, Atmos. Meas. Tech., 6, 1061-1071, 10.5194/amt-6-1061-2013, 2013.

Nie, W., Yan, C., Huang, D. D., Wang, Z., Liu, Y., Qiao, X., Guo, Y., Tian, L., Zheng, P., Xu, Z., Li, Y., Xu, Z., Qi, X., Sun, P., Wang, J., Zheng, F., Li, X., Yin, R., Dallenbach, K. R., Bianchi, F., Petäjä, T., Zhang, Y., Wang, M., Schervish, M., Wang, S., Qiao, L., Wang, Q., Zhou, M., Wang, H., Yu, C., Yao, D., Guo, H., Ye, P., Lee, S., Li, Y. J., Liu, Y., Chi, X., Kerminen, V.-M., Ehn, M., Donahue, N. M., Wang, T., Huang, C., Kulmala, M., Worsnop, D., Jiang, J., and Ding, A.: Secondary organic aerosol formed by condensing anthropogenic vapours over China's megacities, Nature Geoscience, 15, 255-261, 10.1038/s41561-022-00922-5, 2022.

Niu, Y., Yan, Y., Chai, J., Zhang, X., Xu, Y., Duan, X., Wu, J., and Peng, L.: Effects of regional transport from different potential pollution areas on volatile organic compounds (VOCs) in Northern Beijing during non-heating and heating periods, Science of The Total Environment, 836, 155465, https://doi.org/10.1016/j.scitotenv.2022.155465, 2022.

Okuda, T., Matsuura, S., Yamaguchi, D., Umemura, T., Hanada, E., Orihara, H., Tanaka, S., He, K., Ma, Y., Cheng, Y., and Liang, L.: The impact of the pollution control measures for the 2008 Beijing Olympic Games on the chemical composition of aerosols, Atmospheric Environment, 45, 2789-2794, https://doi.org/10.1016/j.atmosenv.2011.01.053, 2011.

Paasonen, P., Nieminen, T., Asmi, E., Manninen, H. E., Petaja, T., Plass-Duelmer, C., Flentje, H., Birmili, W., Wiedensohler, A., Horrak, U., Metzger, A., Hamed, A., Laaksonen, A., Facchini, M. C., Kerminen, V. M., and Kulmala, M.: On the roles of sulphuric acid and low-volatility organic vapours in the initial steps of atmospheric new particle formation, Atmospheric Chemistry and Physics, 10, 11223-11242, 10.5194/acp-10-11223-2010, 2010.

Petäjä, T., Mauldin, I. R. L., Kosciuch, E., McGrath, J., Nieminen, T., Paasonen, P., Boy, M., Adamov, A., Kotiaho, T., and Kulmala, M.: Sulfuric acid and OH concentrations in a boreal forest site, Atmospheric Chemistry and Physics, 9, 7435-7448, 10.5194/acp-9-7435-2009, 2009.

Riedel, T. P., Lin, Y.-H., Budisulistiorini, S. H., Gaston, C. J., Thornton, J. A., Zhang, Z., Vizuete, W., Gold, A., and Surratt, J. D.: Heterogeneous Reactions of Isoprene-Derived Epoxides: Reaction Probabilities and Molar Secondary Organic Aerosol Yield Estimates, Environmental Science & Technology Letters, 2, 38-42, 10.1021/ez500406f, 2015.

Schleicher, N., Norra, S., Chen, Y., Chai, F., and Wang, S.: Efficiency of mitigation measures to reduce particulate air pollution—A case study during the Olympic Summer Games 2008 in Beijing, China, Science of The Total Environment, 427-428, 146-158, https://doi.org/10.1016/j.scitotenv.2012.04.004, 2012.

Shang, D., Peng, J., Guo, S., Wu, Z., and Hu, M.: Secondary aerosol formation in winter haze over the Beijing-Tianjin-Hebei Region, China, Frontiers of Environmental Science & Engineering, 15, 10.1007/s11783-020-1326-x, 2020.

Shi, X., and Brasseur, G. P.: The Response in Air Quality to the Reduction of Chinese Economic Activities during the COVID-19 Outbreak, Geophys Res Lett, e2020GL088070, 10.1029/2020GL088070, 2020.

Shiraiwa, M., Li, Y., Tsimpidi, A. P., Karydis, V. A., Berkemeier, T., Pandis, S. N., Lelieveld, J., Koop, T., and Pöschl, U.: Global distribution of particle phase state in atmospheric secondary organic aerosols, Nature Communications, 8, 15002, 10.1038/ncomms15002, 2017.

Shou-bin, F., Gang, T., Gang, L., Yu-hu, H., Jian-ping, Q., and Shui-yuan, C.: Road fugitive dust emission characteristics in Beijing during Olympics Game 2008 in Beijing, China, Atmospheric Environment, 43, 6003-6010, https://doi.org/10.1016/j.atmosenv.2009.08.028, 2009.

Sipilä, M., Berndt, T., Petäjä, T., Brus, D., Vanhanen, J., Stratmann, F., Patokoski, J., Mauldin Roy, L., Hyvärinen, A.-P., Lihavainen, H., and Kulmala, M.: The Role of Sulfuric Acid in Atmospheric Nucleation, Science, 327, 1243-1246, 10.1126/science.1180315, 2010.

Sun, J., Liu, L., Xu, L., Wang, Y., Wu, Z., Hu, M., Shi, Z., Li, Y., Zhang, X., Chen, J., and Li, W.: Key Role of Nitrate in Phase Transitions of Urban Particles: Implications of Important Reactive Surfaces for Secondary Aerosol Formation, Journal of Geophysical Research: Atmospheres, 123, 1234-1243, https://doi.org/10.1002/2017JD027264, 2018.

Sun, Y., Wang, Z., Fu, P., Jiang, Q., Yang, T., Li, J., and Ge, X.: The impact of relative humidity on aerosol composition and evolution processes during wintertime in Beijing, China, Atmospheric Environment, 77, 927-934, 10.1016/j.atmosenv.2013.06.019, 2013a.

Sun, Y., Jiang, Q., Wang, Z., Fu, P., Li, J., Yang, T., and Yin, Y.: Investigation of the sources and evolution processes of severe haze pollution in Beijing in January 2013, Journal of Geophysical Research, 119, 4380-4398, 10.1002/2014jd021641, 2014.

Sun, Y., Wang, Z., Wild, O., Xu, W., Chen, C., Fu, P., Du, W., Zhou, L., Zhang, Q., Han, T., Wang, Q., Pan, X., Zheng, H., Li, J., Guo, X., Liu, J., and Worsnop, D. R.: "APEC Blue": Secondary Aerosol Reductions from Emission Controls in Beijing, Sci Rep, 6, 20668, 10.1038/srep20668, 2016.

795 Sun, Y., Lei, L., Zhou, W., Chen, C., He, Y., Sun, J., Li, Z., Xu, W., Wang, Q., Ji, D., Fu, P., Wang, Z., and Worsnop, D. R.: A chemical cocktail during the COVID-19 outbreak in Beijing, China: Insights from six-year aerosol particle composition measurements during the Chinese New Year holiday, The Science of the total environment, 742, 140739, 10.1016/j.scitotenv.2020.140739, 2020.

Sun, Y. L., Wang, Z. F., Fu, P. Q., Yang, T., Jiang, Q., Dong, H. B., Li, J., and Jia, J. J.: Aerosol composition, sources and 800 processes during wintertime in Beijing, China, Atmospheric Chemistry and Physics, 13, 4577-4592, 10.5194/acp-13-4577-2013, 2013b.

Sun, Y. L., Wang, Z. F., Du, W., Zhang, Q., Wang, Q. Q., Fu, P. Q., Pan, X. L., Li, J., Jayne, J., and Worsnop, D. R.: Long-term real-time measurements of aerosol particle composition in Beijing, China: seasonal variations, meteorological effects, and source analysis, Atmospheric Chemistry and Physics, 15, 10149-10165, 10.5194/acp-15-10149-2015, 2015.

805 Tan, P.-H., Chou, C., Liang, J.-Y., Chou, C. C. K., and Shiu, C.-J.: Air pollution "holiday effect" resulting from the Chinese New Year, Atmospheric Environment, 43, 2114-2124, https://doi.org/10.1016/j.atmosenv.2009.01.037, 2009.

Tan, Q., Ge, B., Xu, X., Gan, L., Yang, W., Chen, X., Pan, X., Wang, W., Li, J., and Wang, Z.: Increasing impacts of the relative contributions of regional transport on air pollution in Beijing: Observational evidence, Environmental Pollution, 292, 118407, https://doi.org/10.1016/j.envpol.2021.118407, 2022.

810 Tan, Z., Lu, K., Dong, H., Hu, M., Li, X., Liu, Y., Lu, S., Shao, M., Su, R., Wang, H., Wu, Y., Wahner, A., and Zhang, Y.: Explicit diagnosis of the local ozone production rate and the ozone-NO$_x$-VOC sensitivities, Science Bulletin, 63, 1067-1076, https://doi.org/10.1016/j.scib.2018.07.001, 2018.

Trostl, J., Chuang, W. K., Gordon, H., Heinritzi, M., Yan, C., Molteni, U., Ahlm, L., Frege, C., Bianchi, F., Wagner, R., Simon, M., Lehtipalo, K., Williamson, C., Craven, J. S., Duplissy, J., Adamov, A., Almeida, J., Bernhammer, A. K., Breitenlechner, 815 M., Brilke, S., Dias, A., Ehrhart, S., Flagan, R. C., Franchin, A., Fuchs, C., Guida, R., Gysel, M., Hansel, A., Hoyle, C. R., Jokinen, T., Junninen, H., Kangasluoma, J., Keskinen, H., Kim, J., Krapf, M., Kurten, A., Laaksonen, A., Lawler, M., Leiminger, M., Mathot, S., Mohler, O., Nieminen, T., Onnela, A., Petaja, T., Piel, F. M., Miettinen, P., Rissanen, M. P., Rondo, L., Sarnela, N., Schobesberger, S., Sengupta, K., Sipila, M., Smith, J. N., Steiner, G., Tome, A., Virtanen, A., Wagner, A. C., Weingartner, E., Wimmer, D., Winkler, P. M., Ye, P., Carslaw, K. S., Curtius, J., Dommen, J., Kirkby, J., Kulmala, M., Riipinen, I., Worsnop, 820 D. R., Donahue, N. M., and Baltensperger, U.: The role of low-volatility organic compounds in initial particle growth in the atmosphere, Nature, 533, 527-531, 10.1038/nature18271, 2016.

Wang, H., Lu, K., Chen, X., Zhu, Q., Chen, Q., Guo, S., Jiang, M., Li, X., Shang, D., Tan, Z., Wu, Y., Wu, Z., Zou, Q., Zheng, Y., Zeng, L., Zhu, T., Hu, M., and Zhang, Y.: High N2O5 Concentrations Observed in Urban Beijing: Implications of a Large Nitrate Formation Pathway, Environmental Science & Technology Letters, 4, 416-420, 10.1021/acs.estlett.7b00341, 2017.

825 Wang, J., Li, J., Ye, J., Zhao, J., Wu, Y., Hu, J., Liu, D., Nie, D., Shen, F., Huang, X., Huang, D. D., Ji, D., Sun, X., Xu, W., Guo, J., Song, S., Qin, Y., Liu, P., Turner, J. R., Lee, H. C., Hwang, S., Liao, H., Martin, S. T., Zhang, Q., Chen, M., Sun, Y., Ge, X., and Jacob, D. J.: Fast sulfate formation from oxidation of SO2 by NO2 and HONO observed in Beijing haze, Nature communications, 11, 2844, 10.1038/s41467-020-16683-x, 2020a.

Wang, M., Kong, W., Marten, R., He, X. C., Chen, D., Pfeifer, J., Heitto, A., Kontkanen, J., Dada, L., Kurten, A., Yli-Juuti, T., 830 Manninen, H. E., Amanatidis, S., Amorim, A., Baalbaki, R., Baccarini, A., Bell, D. M., Bertozzi, B., Brakling, S., Brilke, S., Murillo, L. C., Chiu, R., Chu, B., De Menezes, L. P., Duplissy, J., Finkenzeller, H., Carracedo, L. G., Granzin, M., Guida, R., Hansel, A., Hofbauer, V., Krechmer, J., Lehtipalo, K., Lamkaddam, H., Lampimaki, M., Lee, C. P., Makhmutov, V., Marie, G., Mathot, S., Mauldin, R. L., Mentler, B., Muller, T., Onnela, A., Partoll, E., Petaja, T., Philippov, M., Pospisilova, V., Ranjithkumar, A., Rissanen, M., Rorup, B., Scholz, W., Shen, J., Simon, M., Sipila, M., Steiner, G., Stolzenburg, D., Tham, Y. 835 J., Tome, A., Wagner, A. C., Wang, D. S., Wang, Y., Weber, S. K., Winkler, P. M., Wlasits, P. J., Wu, Y., Xiao, M., Ye, Q., Zauner-Wieczorek, M., Zhou, X., Volkamer, R., Riipinen, I., Dommen, J., Curtius, J., Baltensperger, U., Kulmala, M., Worsnop, D. R., Kirkby, J., Seinfeld, J. H., El-Haddad, I., Flagan, R. C., and Donahue, N. M.: Rapid growth of new atmospheric particles by nitric acid and ammonia condensation, Nature, 581, 184-189, 10.1038/s41586-020-2270-4, 2020b.

Wang, S., Zhao, M., Xing, J., Wu, Y., Zhou, Y., Lei, Y., He, K., Fu, L., and Hao, J.: Quantifying the Air Pollutants Emission Reduction during the 2008 Olympic Games in Beijing, Environ. Sci. Technol., 44, 2490-2496, 10.1021/es9028167, 2010.

Wang, Y., Wang, Q., Ye, J., Yan, M., Qin, Q., Prévôt, A. S. H., and Cao, J.: A Review of Aerosol Chemical Composition and Sources in Representative Regions of China during Wintertime, Atmosphere, 10, 10.3390/atmos10050277, 2019.

Wang, Y., Chen, Y., Wu, Z., Shang, D., Bian, Y., Du, Z., Schmitt, S. H., Su, R., Gkatzelis, G. I., Schlag, P., Hohaus, T., Voliotis, A., Lu, K., Zeng, L., Zhao, C., Alfarra, M. R., McFiggans, G., Wiedensohler, A., Kiendler-Scharr, A., Zhang, Y., and Hu, M.: Mutual promotion between aerosol particle liquid water and particulate nitrate enhancement leads to severe nitrate-dominated particulate matter pollution and low visibility, Atmospheric Chemistry and Physics, 20, 2161-2175, 10.5194/acp-20-2161-2020, 2020c.

Wang, Y., Gao, W., Wang, S., Song, T., Gong, Z., Ji, D., Wang, L., Liu, Z., Tang, G., Huo, Y., Tian, S., Li, J., Li, M., Yang, Y., Chu, B., Petäjä, T., Kerminen, V.-M., He, H., Hao, J., Kulmala, M., Wang, Y., and Zhang, Y.: Contrasting trends of $PM_{2.5}$ and surface-ozone concentrations in China from 2013 to 2017, National Science Review, 7, 1331-1339, 10.1093/nsr/nwaa032, 2020d.

Wang, Z. B., Hu, M., Wu, Z. J., Yue, D. L., He, L. Y., Huang, X. F., Liu, X. G., and Wiedensohler, A.: Long-term measurements of particle number size distributions and the relationships with air mass history and source apportionment in the summer of Beijing, Atmos. Chem. Phys., 13, 10159-10170, 10.5194/acp-13-10159-2013, 2013.

Wilson, J., Imre, D., Beránek, J., Shrivastava, M., and Zelenyuk, A.: Evaporation Kinetics of Laboratory-Generated Secondary Organic Aerosols at Elevated Relative Humidity, Environmental Science & Technology, 49, 243-249, 10.1021/es505331d, 2015.

Xiao, C., Chang, M., Guo, P., Gu, M., and Li, Y.: Analysis of air quality characteristics of Beijing-Tianjin-Hebei and its surrounding air pollution transport channel cities in China, J Environ Sci (China), 87, 213-227, 10.1016/j.jes.2019.05.024, 2020.

Xie, Y., Wang, G., Wang, X., Chen, J., Chen, Y., Tang, G., Wang, L., Ge, S., Xue, G., Wang, Y., and Gao, J.: Nitrate-dominated $PM_{2.5}$ and elevation of particle pH observed in urban Beijing during the winter of 2017, Atmospheric Chemistry and Physics, 20, 5019-5033, 10.5194/acp-20-5019-2020, 2020.

Xu, G., Wang, C., Xu, C., and Bai, P.: Evaluation of air pollutant emissions from scattered coal burning and electric heating in Beijing-Tianjin-Hebei region, Research of Environmental Sciences, 29, 1735-1742, 2016.

Xu, Q., Wang, S., Jiang, J., Bhattarai, N., Li, X., Chang, X., Qiu, X., Zheng, M., Hua, Y., and Hao, J.: Nitrate dominates the chemical composition of PM2.5 during haze event in Beijing, China, Sci Total Environ, 689, 1293-1303, 10.1016/j.scitotenv.2019.06.294, 2019.

Xu, W. Q., Han, T. T., Du, W., Wang, Q. Q., Chen, C., Zhao, J., Zhang, Y. J., Li, J., Fu, P. Q., Wang, Z. F., Worsnop, D. R., and Sun, Y. L.: Effects of Aqueous-Phase and Photochemical Processing on Secondary Organic Aerosol Formation and Evolution in Beijing, China, Environ. Sci. Technol., 51, 762-770, 10.1021/acs.est.6b04498, 2017.

Xue, J., Yuan, Z. B., Lau, A. K. H., and Yu, J. Z.: Insights into factors affecting nitrate in PM2.5 in a polluted high NOx environment through hourly observations and size distribution measurements, J. Geophys. Res.-Atmos., 119, 4888-4902, 10.1002/2013jd021108, 2014.

Yan, C., Yin, R., Lu, Y., Dada, L., Yang, D., Fu, Y., Kontkanen, J., Deng, C., Garmash, O., Ruan, J., Baalbaki, R., Schervish, M., Cai, R., Bloss, M., Chan, T., Chen, T., Chen, Q., Chen, X., Chen, Y., Chu, B., Dällenbach, K., Foreback, B., He, X., Heikkinen, L., Jokinen, T., Junninen, H., Kangasluoma, J., Kokkonen, T., Kurppa, M., Lehtipalo, K., Li, H., Li, H., Li, X., Liu, Y., Ma, Q., Paasonen, P., Rantala, P., Pileci, R. E., Rusanen, A., Sarnela, N., Simonen, P., Wang, S., Wang, W., Wang, Y., Xue, M., Yang, G., Yao, L., Zhou, Y., Kujansuu, J., Petäjä, T., Nie, W., Ma, Y., Ge, M., He, H., Donahue, N. M., Worsnop, D. R., Veli-Matti, K., Wang, L., Liu, Y., Zheng, J., Kulmala, M., Jiang, J., and Bianchi, F.: The synergistic role of sulfuric acid, bases, and oxidized organics governing new-particle formation in Beijing, Geophysical Research Letters, 48, e2020GL091944, https://doi.org/10.1029/2020GL091944, 2021.

Yan, C., Shen, Y., Stolzenburg, D., Dada, L., Qi, X., Hakala, S., Sundström, A. M., Guo, Y., Lipponen, A., Kokkonen, T., Kontkanen, J., Cai, R., Cai, J., Chan, T., Chen, L., Chu, B., Deng, C., Du, W., Fan, X., He, X. C., Kangasluoma, J., Kujansuu, J., Kurppa, M., Li, C., Li, Y., Lin, Z., Liu, Y., Liu, Y., Lu, Y., Nie, W., Pulliainen, J., Qiao, X., Wang, Y., Wen, Y., Wu, Y., Yang, G., Yao, L., Yin, R., Zhang, G., Zhang, S., Zheng, F., Zhou, Y., Arola, A., Tamminen, J., Paasonen, P., Sun, Y., Wang, L., Donahue, N. M., Liu, Y., Bianchi, F., Daellenbach, K. R., Worsnop, D. R., Kerminen, V. M., Petäjä, T., Ding, A., Jiang, J.,

and Kulmala, M.: The effect of COVID-19 restrictions on atmospheric new particle formation in Beijing, Atmos. Chem. Phys. Discuss., 2022, 1-24, 10.5194/acp-2021-1079, 2022.

890   Yang, L., Nie, W., Liu, Y., Xu, Z., Xiao, M., Qi, X., Li, Y., Wang, R., Zou, J., Paasonen, P., Yan, C., Xu, Z., Wang, J., Zhou, C., Yuan, J., Sun, J., Chi, X., Kerminen, V.-M., Kulmala, M., and Ding, A.: Toward building a physical proxy for gas-phase sulfuric acid concentration based on its budget analysis in polluted Yangtze River Delta, East China, Environmental Science & Technology, 55, 6665-6676, 10.1021/acs.est.1c00738, 2021.

Yao, D., Tang, G., Wang, Y., Yang, Y., Wang, L., Chen, T., He, H., and Wang, Y.: Significant contribution of spring northwest transport to volatile organic compounds in Beijing, Journal of Environmental Sciences, 104, 169-181,
895   https://doi.org/10.1016/j.jes.2020.11.023, 2021.

Yao, D., Tang, G., Sun, J., Wang, Y., Yang, Y., Wang, Y., Liu, B., He, H., and Wang, Y.: Annual nonmethane hydrocarbon trends in Beijing from 2000 to 2019, Journal of Environmental Sciences, 112, 210-217,
https://doi.org/10.1016/j.jes.2021.04.017, 2022.

Yao, L., Garmash, O., Bianchi, F., Zheng, J., Yan, C., Kontkanen, J., Junninen, H., Mazon, S. B., Ehn, M., Paasonen, P., Sipila,
900   M., Wang, M. Y., Wang, X. K., Xiao, S., Chen, H. F., Lu, Y. Q., Zhang, B. W., Wang, D. F., Fu, Q. Y., Geng, F. H., Li, L., Wang, H. L., Qiao, L. P., Yang, X., Chen, J. M., Kerminen, V. M., Petaja, T., Worsnop, D. R., Kulmala, M., and Wang, L.: Atmospheric new particle formation from sulfuric acid and amines in a Chinese megacity, Science, 361, 278-281, 10.1126/science.aao4839, 2018.

Yli-Juuti, T., Pajunoja, A., Tikkanen, O.-P., Buchholz, A., Faiola, C., Väisänen, O., Hao, L., Kari, E., Peräkylä, O., Garmash,
905   O., Shiraiwa, M., Ehn, M., Lehtinen, K., and Virtanen, A.: Factors controlling the evaporation of secondary organic aerosol from α-pinene ozonolysis, Geophysical Research Letters, 44, 2562-2570, https://doi.org/10.1002/2016GL072364, 2017.

Yue, D. L., Hu, M., Zhang, R. Y., Wang, Z. B., Zheng, J., Wu, Z. J., Wiedensohler, A., He, L. Y., Huang, X. F., and Zhu, T.: The roles of sulfuric acid in new particle formation and growth in the mega-city of Beijing, Atmospheric Chemistry and Physics, 10, 4953-4960, 10.5194/acp-10-4953-2010, 2010.

910   Zhang, R., Wang, G., Guo, S., Zamora, M. L., Ying, Q., Lin, Y., Wang, W., Hu, M., and Wang, Y.: Formation of urban fine particulate matter, Chemical Reviews, 115, 3803-3855, 10.1021/acs.chemrev.5b00067, 2015.

Zhang, Y., Vu, T. V., Sun, J., He, J., Shen, X., Lin, W., Zhang, X., Zhong, J., Gao, W., Wang, Y., Fu, T. M., Ma, Y., Li, W., and Shi, Z.: Significant Changes in Chemistry of Fine Particles in Wintertime Beijing from 2007 to 2017: Impact of Clean Air Actions, Environ Sci Technol, 54, 1344-1352, 10.1021/acs.est.9b04678, 2020.

915   Zhao, J., Du, W., Zhang, Y., Wang, Q., Chen, C., Xu, W., Han, T., Wang, Y., Fu, P., Wang, Z., Li, Z., and Sun, Y.: Insights into aerosol chemistry during the 2015 China Victory Day parade: results from simultaneous measurements at ground level and 260 m in Beijing, Atmospheric Chemistry and Physics, 17, 3215-3232, 10.5194/acp-17-3215-2017, 2017.

Zhao, J., Qiu, Y., Zhou, W., Xu, W., Wang, J., Zhang, Y., Li, L., Xie, C., Wang, Q., Du, W., Worsnop, D. R., Canagaratna, M. R., Zhou, L., Ge, X., Fu, P., Li, J., Wang, Z., Donahue, N. M., and Sun, Y.: Organic Aerosol Processing During Winter Severe
920   Haze Episodes in Beijing, Journal of Geophysical Research: Atmospheres, 124, 10248-10263, 10.1029/2019jd030832, 2019.

Zhao, S., Yin, D., Yu, Y., Kang, S., Qin, D., and Dong, L.: PM$_{2.5}$ and O$_3$ pollution during 2015–2019 over 367 Chinese cities: Spatiotemporal variations, meteorological and topographical impacts, Environmental Pollution, 264, 114694,
https://doi.org/10.1016/j.envpol.2020.114694, 2020.

Zhao, Z., Zhou, Z., Russo, A., Du, H., Xiang, J., Zhang, J., and Zhou, C.: Impact of meteorological conditions at multiple scales
925   on ozone concentration in the Yangtze River Delta, Environmental Science and Pollution Research, 28, 62991-63007, 10.1007/s11356-021-15160-2, 2021.

Zheng, G. J., Duan, F. K., Su, H., Ma, Y. L., Cheng, Y., Zheng, B., Zhang, Q., Huang, T., Kimoto, T., Chang, D., Pöschl, U., Cheng, Y. F., and He, K. B.: Exploring the severe winter haze in Beijing: the impact of synoptic weather, regional transport and heterogeneous reactions, Atmospheric Chemistry and Physics, 15, 2969-2983, 10.5194/acp-15-2969-2015, 2015.

930   Zhong, J., Zhang, X., Dong, Y., Wang, Y., Liu, C., Wang, J., Zhang, Y., and Che, H.: Feedback effects of boundary-layer meteorological factors on cumulative explosive growth of PM$_{2.5}$ during winter heavy pollution episodes in Beijing from 2013 to 2016, Atmos. Chem. Phys., 18, 247-258, 10.5194/acp-18-247-2018, 2018.

Zhou, W., Gao, M., He, Y., Wang, Q., Xie, C., Xu, W., Zhao, J., Du, W., Qiu, Y., Lei, L., Fu, P., Wang, Z., Worsnop, D. R., Zhang, Q., and Sun, Y.: Response of aerosol chemistry to clean air action in Beijing, China: Insights from two-year ACSM measurements and model simulations, Environmental pollution, 255, 113345, 10.1016/j.envpol.2019.113345, 2019.

Zhou, Y., Dada, L., Liu, Y., Fu, Y., Kangasluoma, J., Chan, T., Yan, C., Chu, B., Daellenbach, K. R., Bianchi, F., Kokkonen, T. V., Liu, Y., Kujansuu, J., Kerminen, V. M., Petäjä, T., Wang, L., Jiang, J., and Kulmala, M.: Variation of size-segregated particle number concentrations in wintertime Beijing, Atmos. Chem. Phys., 20, 1201-1216, 10.5194/acp-20-1201-2020, 2020.

Zhu, Y., Hu, Q., Gao, M., Zhao, C., Zhang, C., Liu, T., Tian, Y., Yan, L., Su, W., Hong, X., and Liu, C.: Quantifying Contributions of Local Emissions and Regional Transport to NO_x in Beijing Using TROPOMI Constrained WRF-Chem Simulation, in: Remote Sensing, 9, 2021.

Tables

Table 1. Division of different periods from 2019 to 2022.

Periods of Four-Year Variability			Periods of Special Event		
Name	Date	Number of Days	Name	Date	Number of Days
2019	01/01 - 01/22, 2019	22	Reference	02/11 - 02/20, 2019 02/04 - 02/10, 2021 02/18 - 02/20, 2021	20
2020	01/01 - 01/22, 2020	22	COVID	02/04 - 02/20, 2020	17
2021	01/01 - 01/22, 2021	22	Olympics	02/04 - 02/20, 2022	17
2022	01/01 - 01/22, 2022	22	CNY	02/04 - 02/10, 2019 02/11 - 02/17, 2021	14

945

Figure Legends
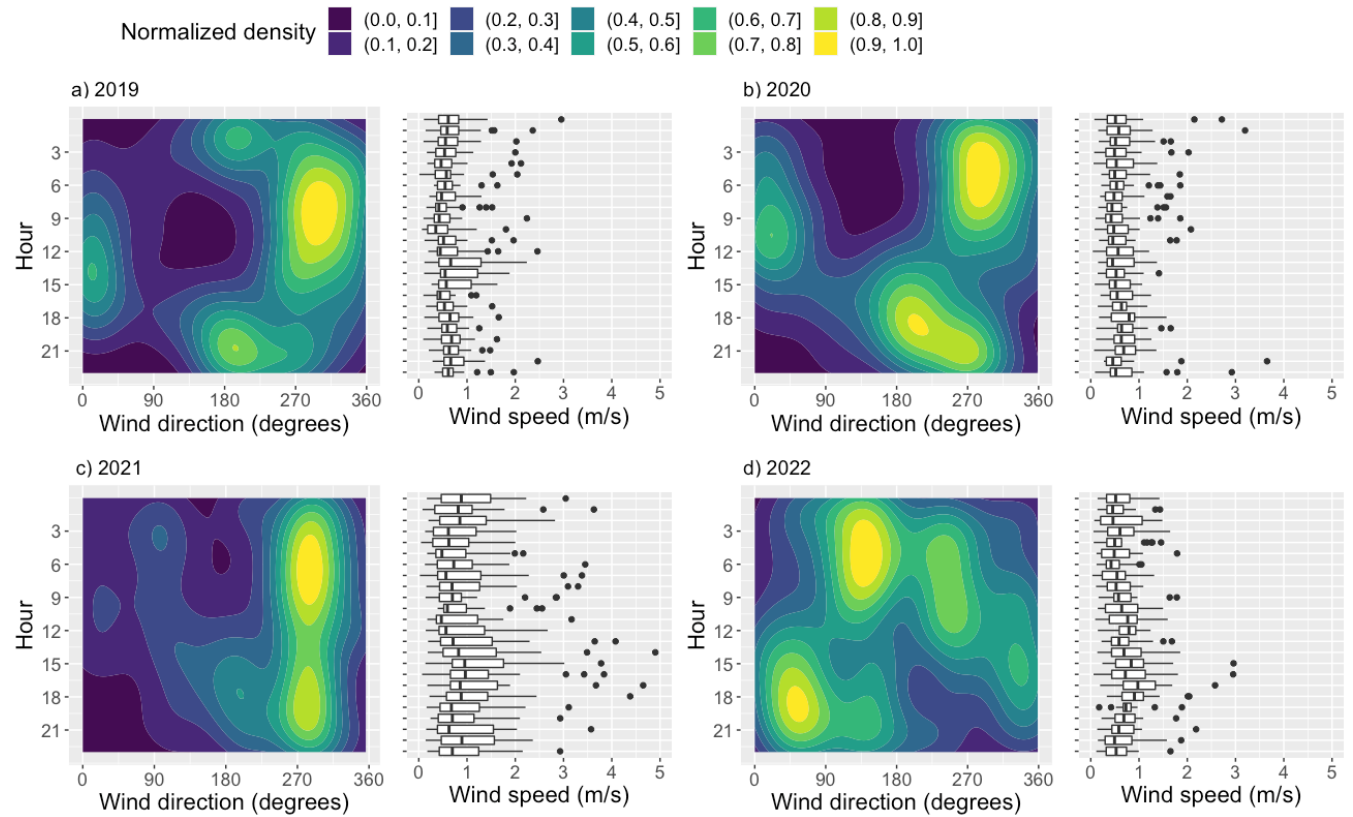
Figure 1. Diurnal variations of wind direction (left panels) and wind speed (right panels) for different years (1st to 22nd January). The wind direction and wind speed are depicted in wind contour plots and boxplots respectively.

950
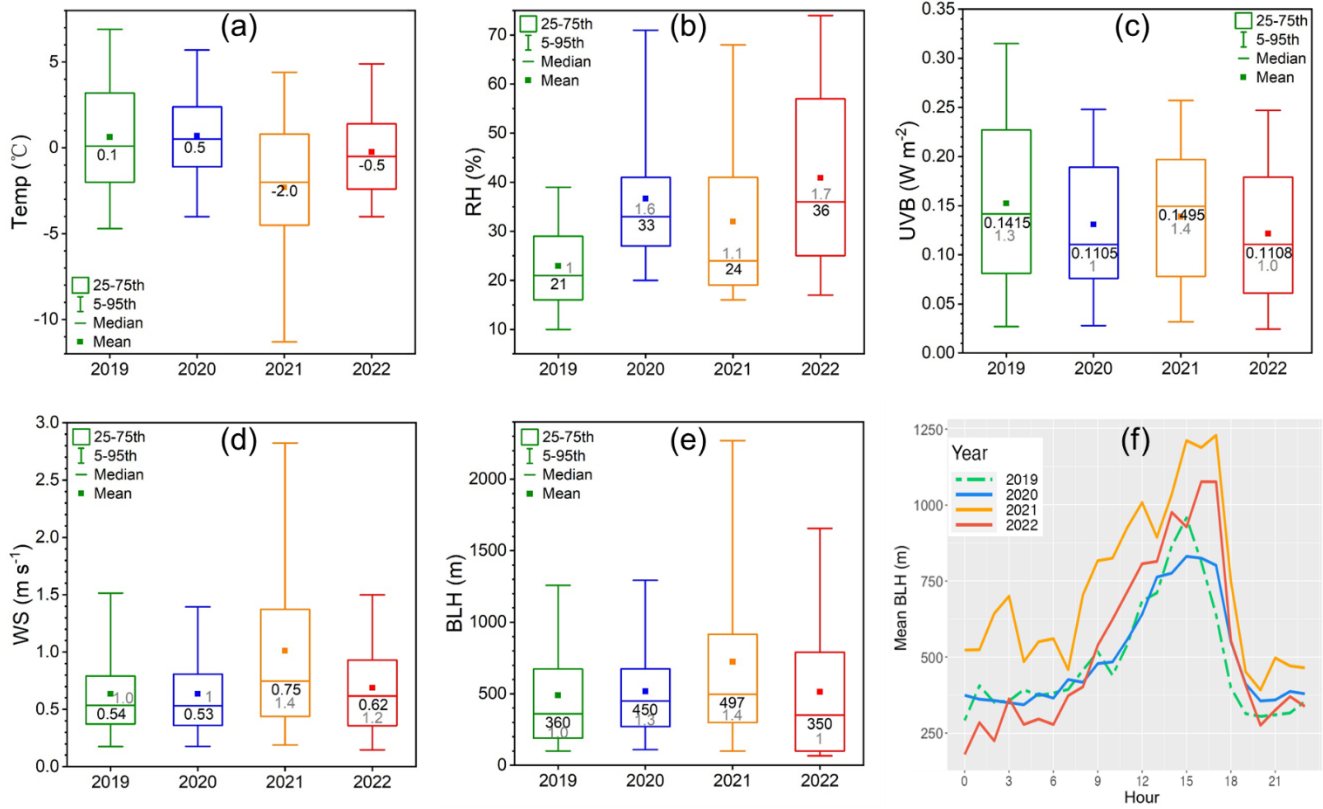
Figure 2. (a) Temperature (Temp), (b) relatively humidity (RH), (c) UVB, (d) wind speed (WS) and (e) boundary layer height (BLH) for different years (1st to 22nd January). (f) Averaged diurnal variations of boundary layer height (BLH) for different years (1st to 22nd January). The black value inside each box is the median value of corresponding parameter. The gray values are the normalized median values to the lowest median value in each subplot, which is used for quantitative variation comparison between different parameters. Please note that for UVB, only daytime (08:00 – 16:00) dataset was used.

955
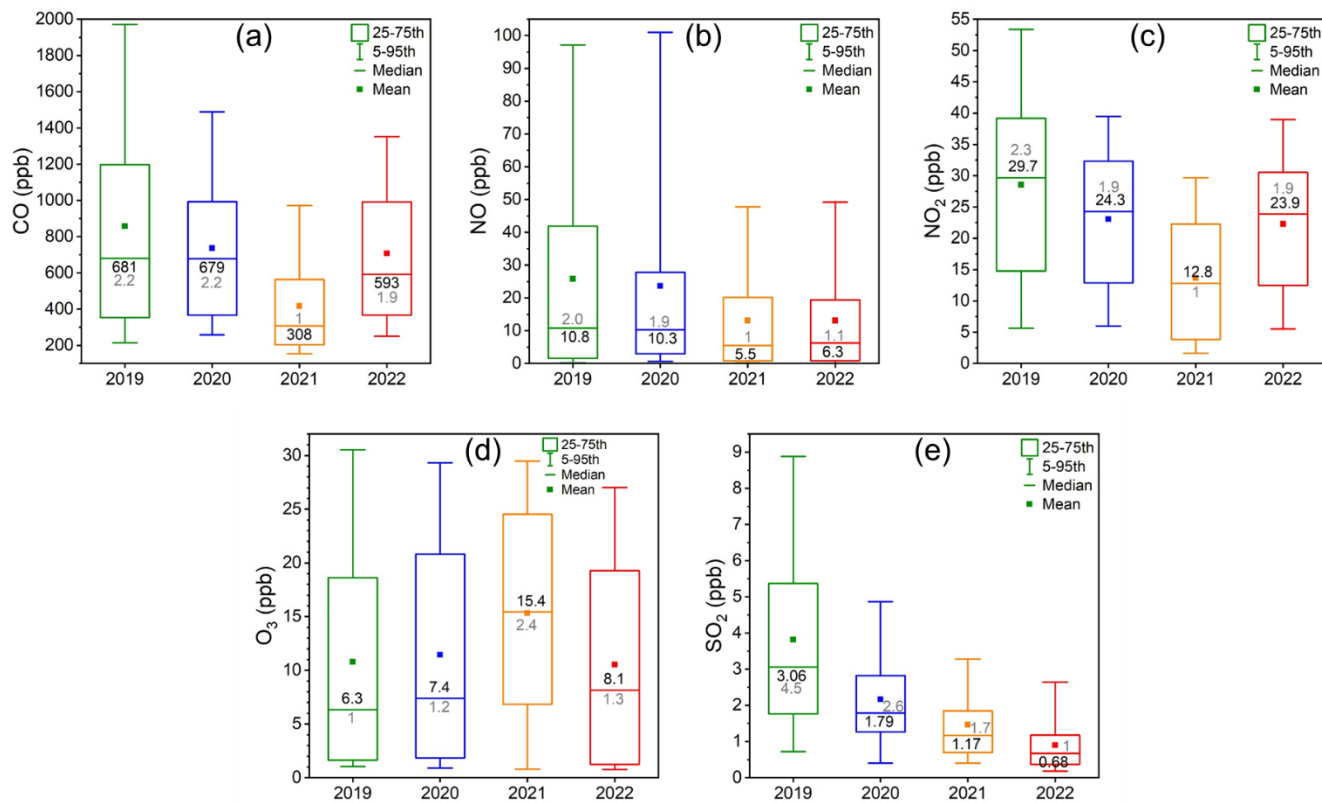
Figure 3. Mixing ratios of (a) CO, (b) NO, (c) NO$_2$, (d) O$_3$ and (e) SO$_2$ for different years (1st to 22nd January). The black value inside each box is the median value of corresponding parameter. The gray values are the normalized median values to the lowest median value in each subplot, which is used for quantitative variation comparison between different parameters.
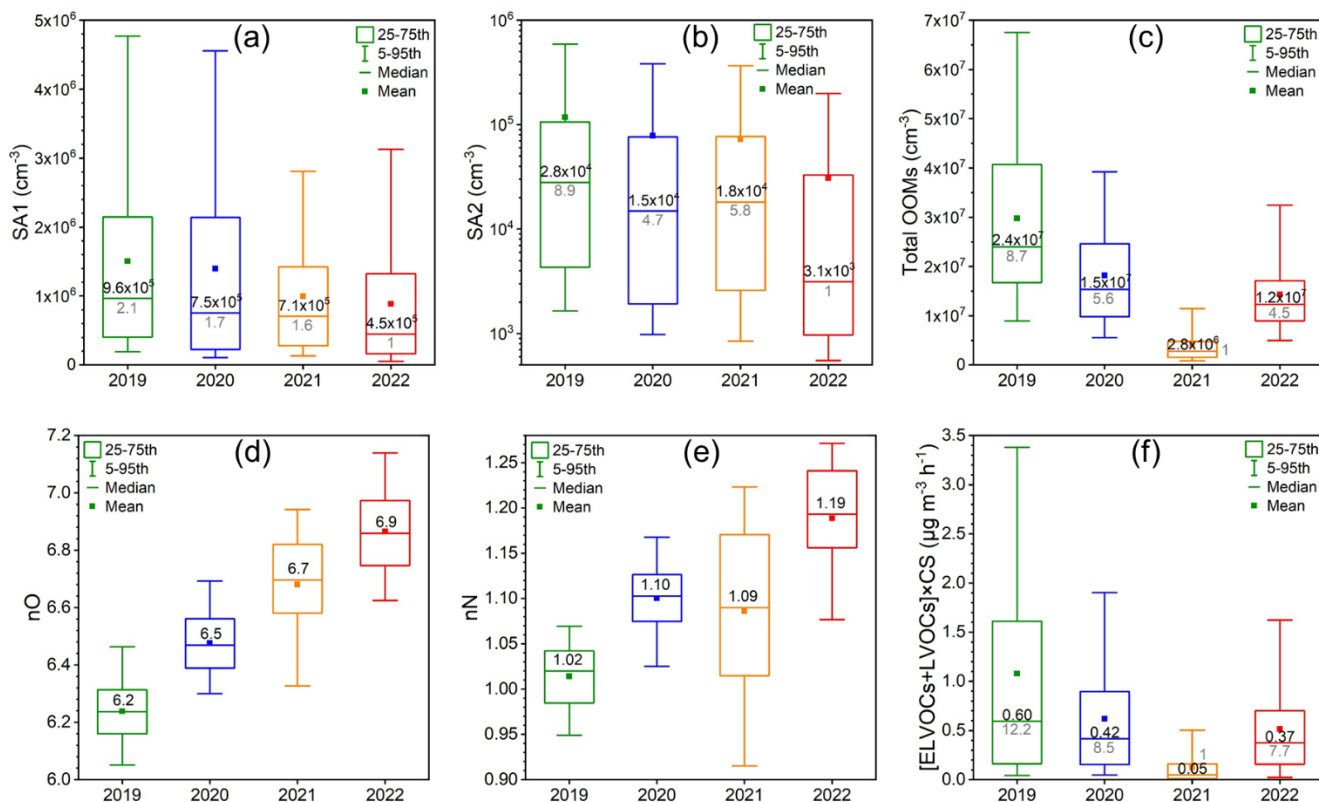
Figure 4. (a) Concentration of sulfuric acid monomer (SA1), (b) concentration of sulfuric acid dimer (SA2), (c) concentration of total OOMs, (d) fraction weighted oxygen number of OOMs (nO), (e) fraction weighted nitrogen number of OOMs (nN) and (f) [ELVOCs+LVOCs]×CS for different years (1st to 22nd January). The black value inside each box is the median value of corresponding parameter. The gray values are the normalized median values to the lowest median value in each subplot, which is used for quantitative variation comparison between different parameters.
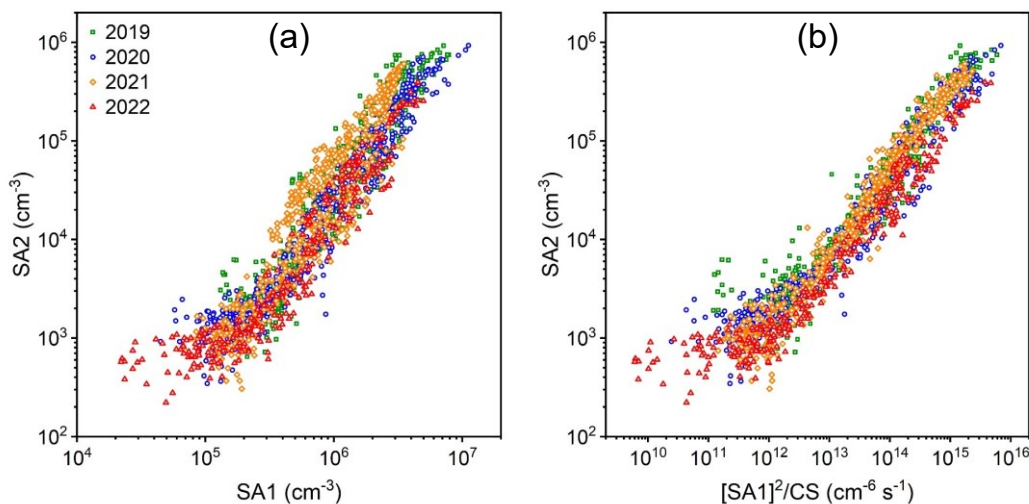
Figure 5. Sulfuric acid dimer (SA2) vs. (a) sulfuric acid monomer (SA1) and (b) [SA1]^2/CS from 2019 to 2022 (1st to 22nd January).
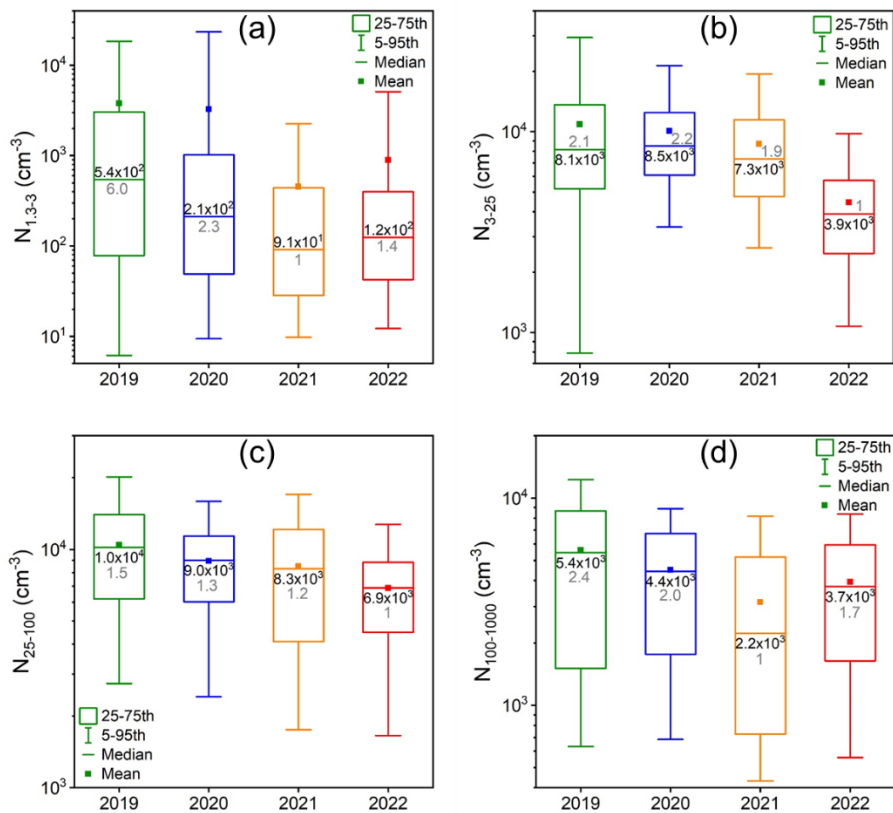
Figure 6. Number concentration of (a) sub-3 nm particles ($N_{1.3-3}$), (b) 3-25 nm particles (N_{3-25}), (c) 25-100 nm particles (N_{25-100}) and (d) 100-1000 nm particles ($N_{100-1000}$) for different years (1st to 22nd January). The black value inside each box is the median value of corresponding parameter. The gray values are the normalized median values to the lowest median value in each subplot, which is used for quantitative variation comparison between different parameters.
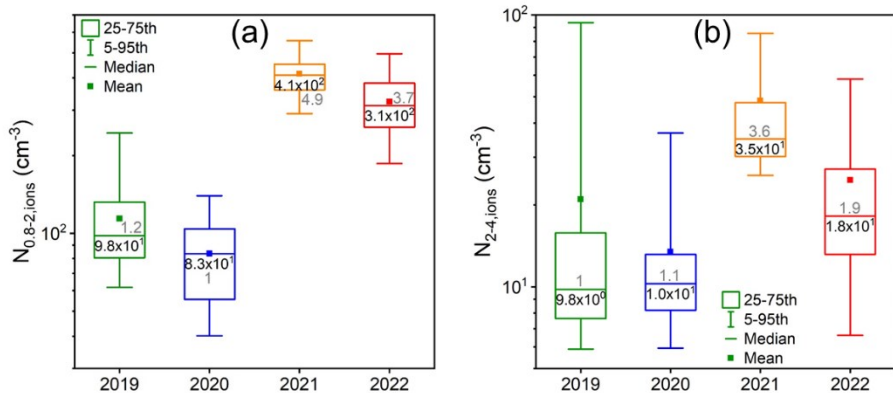
Figure 7. Number concentration of (a) 0.8-2 nm ($N_{0.8-2,\ ions}$) and (b) 2-4 nm ($N_{2-4,\ ions}$) positive ions measured by NAIS for different years (1st to 22nd January). The black value inside each box is the median value of corresponding parameter. The gray values are the normalized median values to the lowest median value in each subplot, which is used for quantitative variation comparison between different parameters.
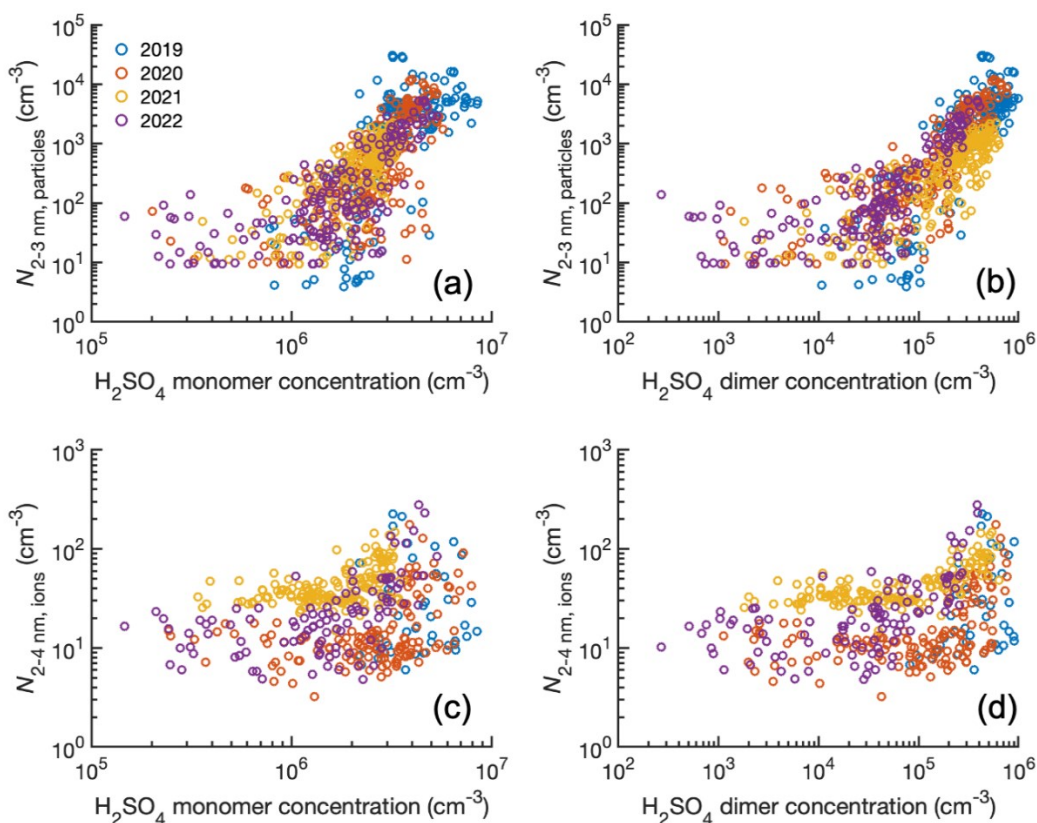
Figure 8. The relations (a) between particle number concentration in 2-3 nm size range and H$_2$SO$_4$ monomer concentration, (b) between particle number concentration in 2-3 nm size range and H$_2$SO$_4$ dimer concentration, (c) between ion number concentration in 2-4 nm size range and H$_2$SO$_4$ monomer concentration and (d) between ion number concentration in 2-4 nm size range and H$_2$SO$_4$ dimer concentration for different years (1st to 22nd January).
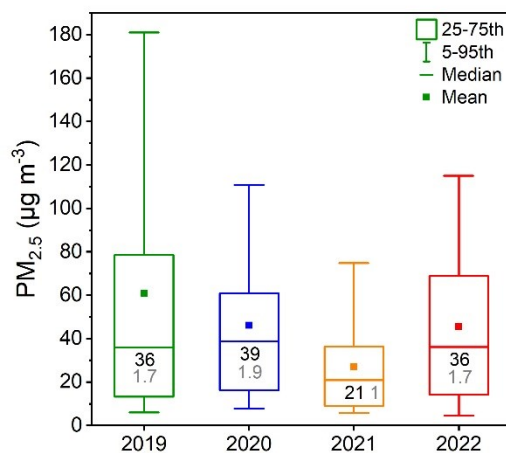
Figure 9. PM$_{2.5}$ mass concentration for different years (1st to 22nd January). The black value inside each box is the median value of corresponding parameter. The gray values are the normalized median values to the lowest median value in each subplot, which is used for quantitative variation comparison between different parameters.
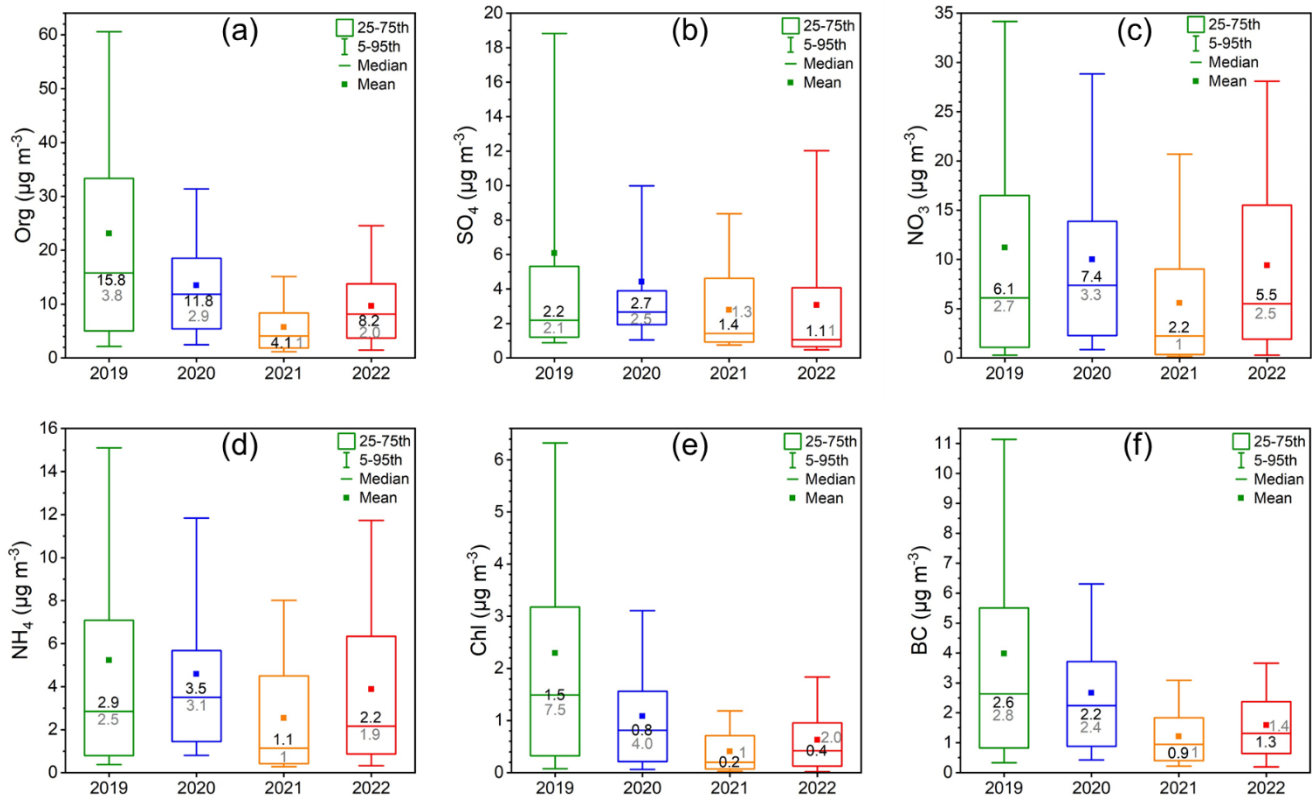
Figure 10. Mass concentrations of PM$_{2.5}$ compositions including (a) organics (Org), (b) sulfate (SO$_4$), (c) nitrate (NO$_3$), (d) ammonium (NH$_4$), (e) chloride (Chl), and (f) black carbon (BC) for different years (1st to 22nd January). The black value inside each box is the median value of corresponding parameter. The gray values are the normalized median values to the lowest median value in each subplot, which is used for quantitative variation comparison between different parameters.
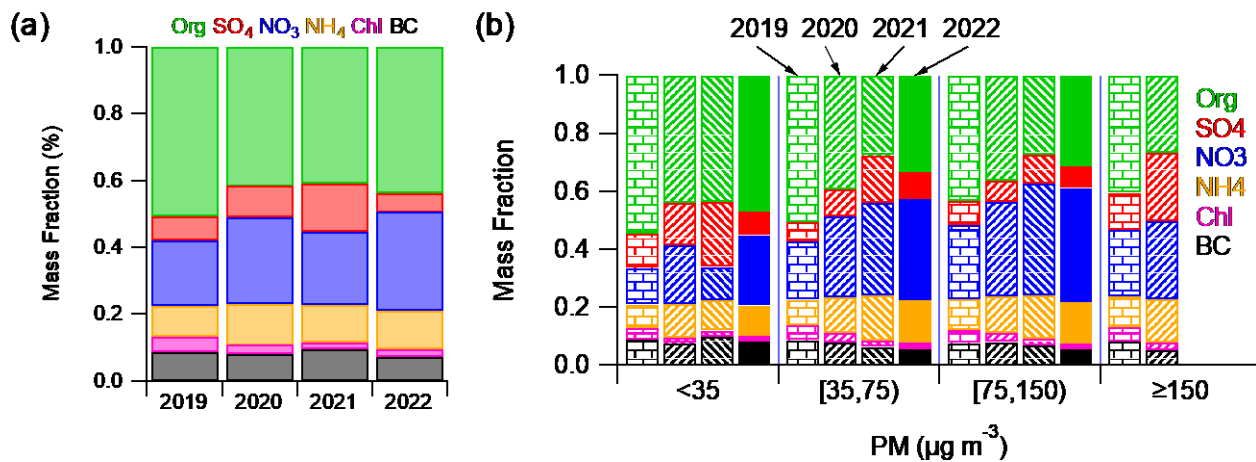
Figure 11. Contributions of PM$_{2.5}$ compositions including organics (Org), sulfate (SO$_4$), nitrate (NO$_3$), ammonium (NH$_4$), chloride (Chl), and black carbon (BC) (a) for different years (1st to 22nd January), and (b) under different PM$_{2.5}$ levels.
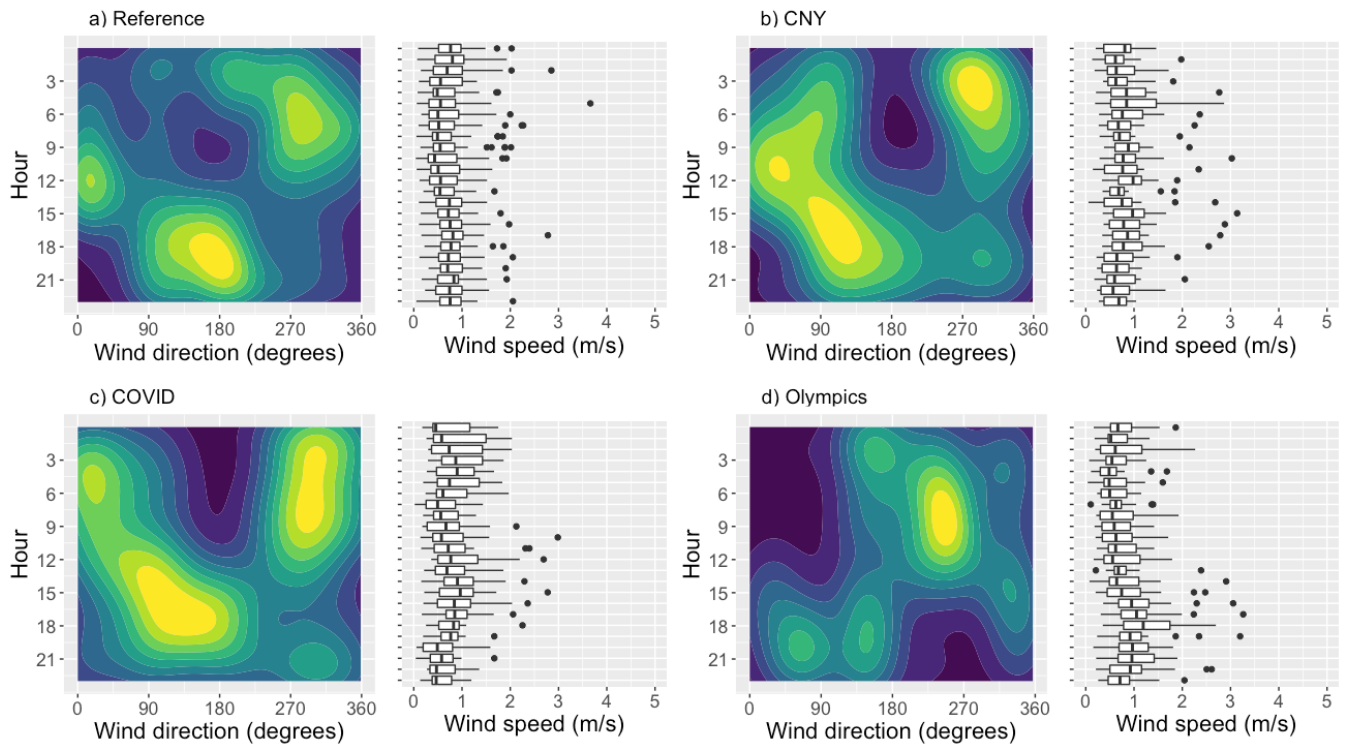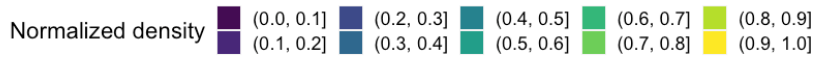
Figure 12. Diurnal variations of wind direction (left panels) and wind speed (right panels) for reference, COVID, Olympics and CNY periods. The wind direction and wind speed are depicted in wind contour plots and boxplots respectively.

1010
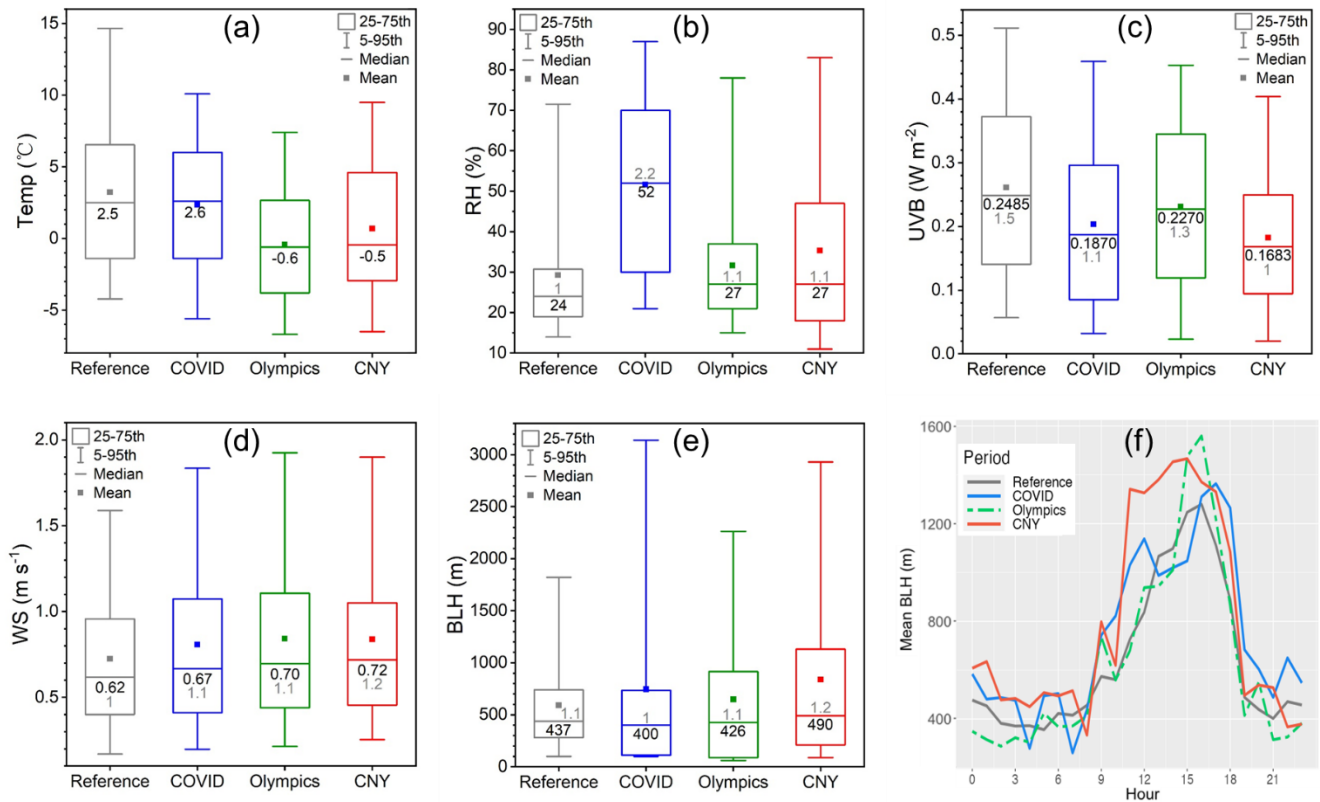
Figure 13. (a) Temperature (Temp), (b) relatively humidity (RH), (c) UVB, (d) wind speed (WS) and (e) boundary layer height (BLH) for reference, COVID, Olympics and CNY periods. (f) Averaged diurnal variations of boundary layer height (BLH) for reference, COVID, Olympics and CNY periods. The black value inside each box is the median value of corresponding parameter. The gray values are the normalized median values to the lowest median value in each subplot, which is used for quantitative variation comparison between different parameters. Please note that for UVB, only daytime (08:00 – 16:00) dataset was used.

1020
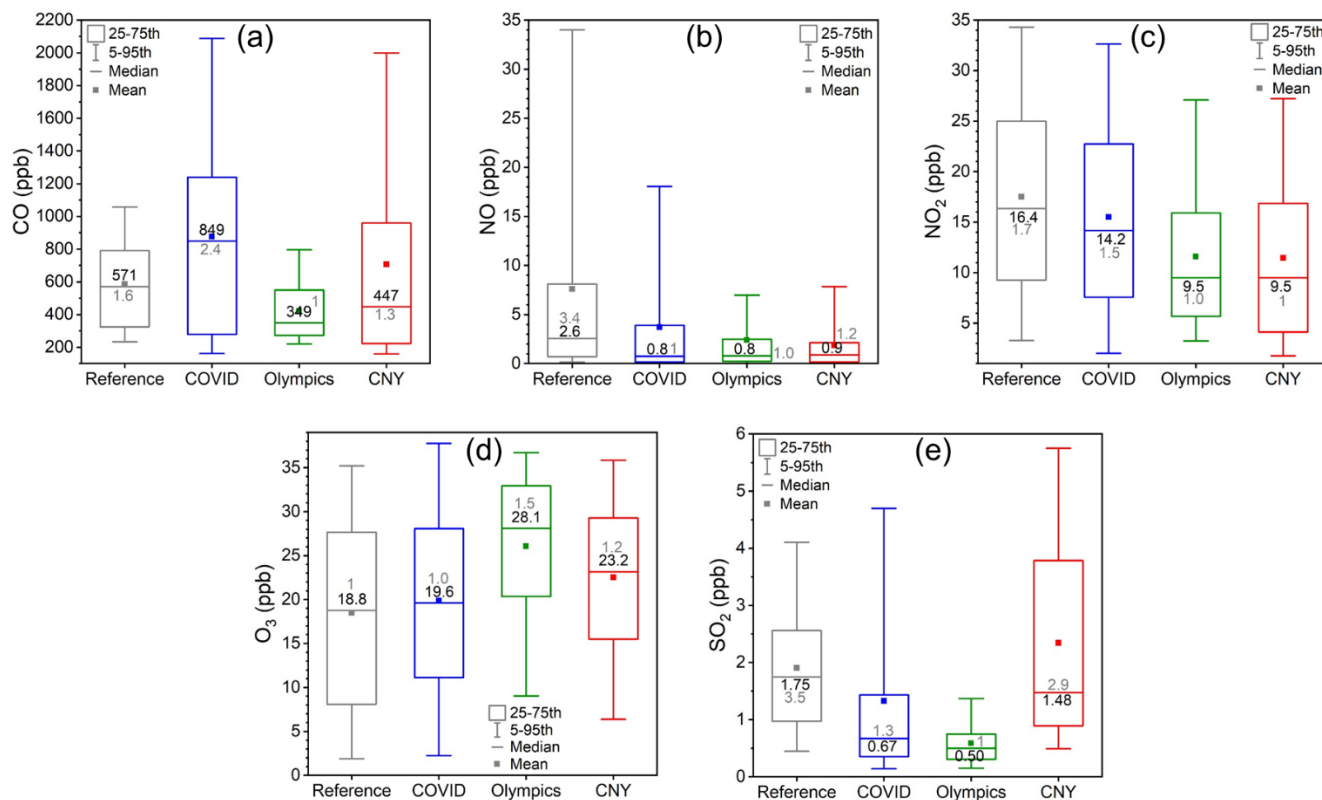
Figure 14. Mixing ratios of (a) CO, (b) NO, (c) NO_2, (d) O_3 and (e) SO_2 for reference, COVID, Olympics and CNY periods. The black value inside each box is the median value of corresponding parameter. The gray values are the normalized median values to the lowest median value in each subplot, which is used for quantitative variation comparison between different parameters.

1025
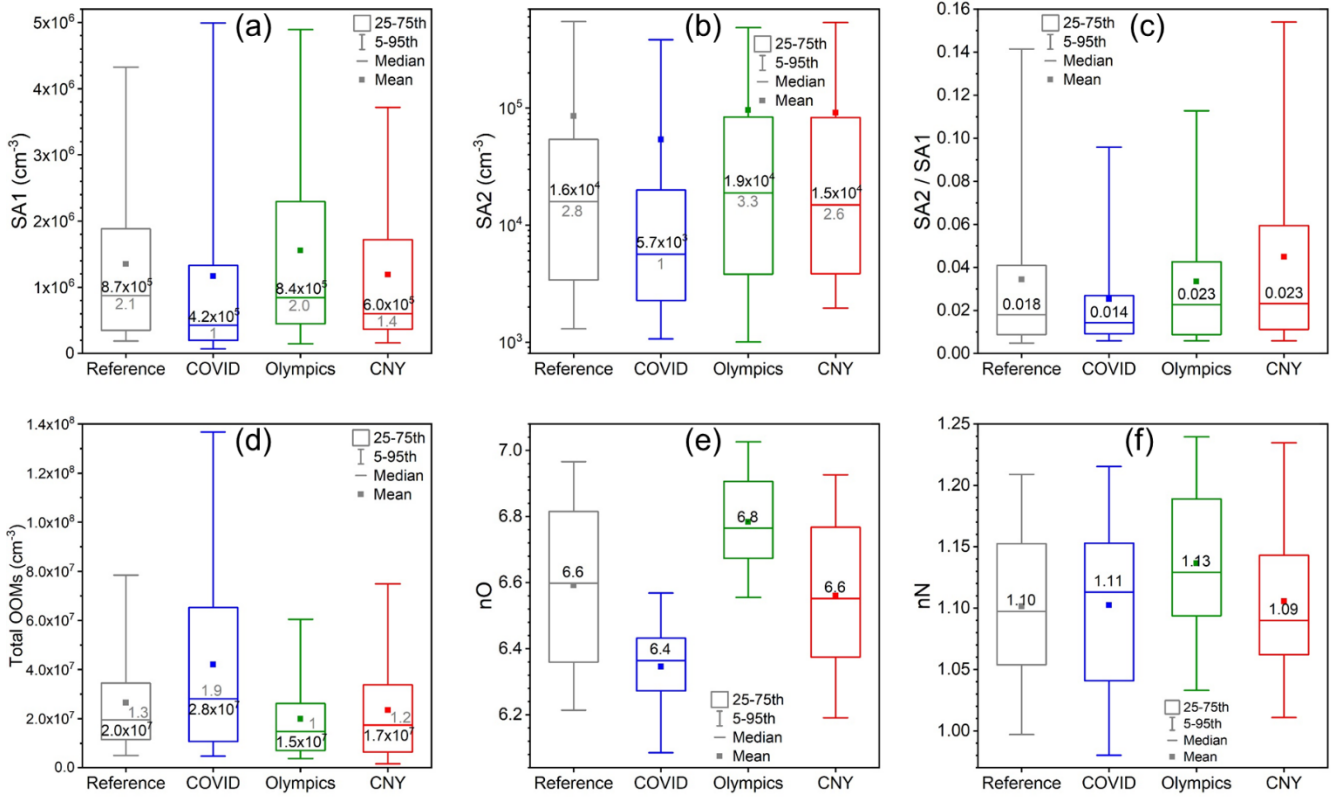
Figure 15. (a) Concentration of sulfuric acid monomer (SA1), (b) concentration of sulfuric acid dimer (SA2), (c) ratio of SA2 to SA1, (d) concentration of total OOMs, (e) fraction weighted oxygen number of OOMs (nO), and (f) fraction weighted nitrogen number of OOMs (nN) for reference, COVID, Olympics and CNY periods. The black value inside each box is the median value of corresponding parameter. The gray values are the normalized median values to the lowest median value in each subplot, which is used for quantitative variation comparison between different parameters.

1030
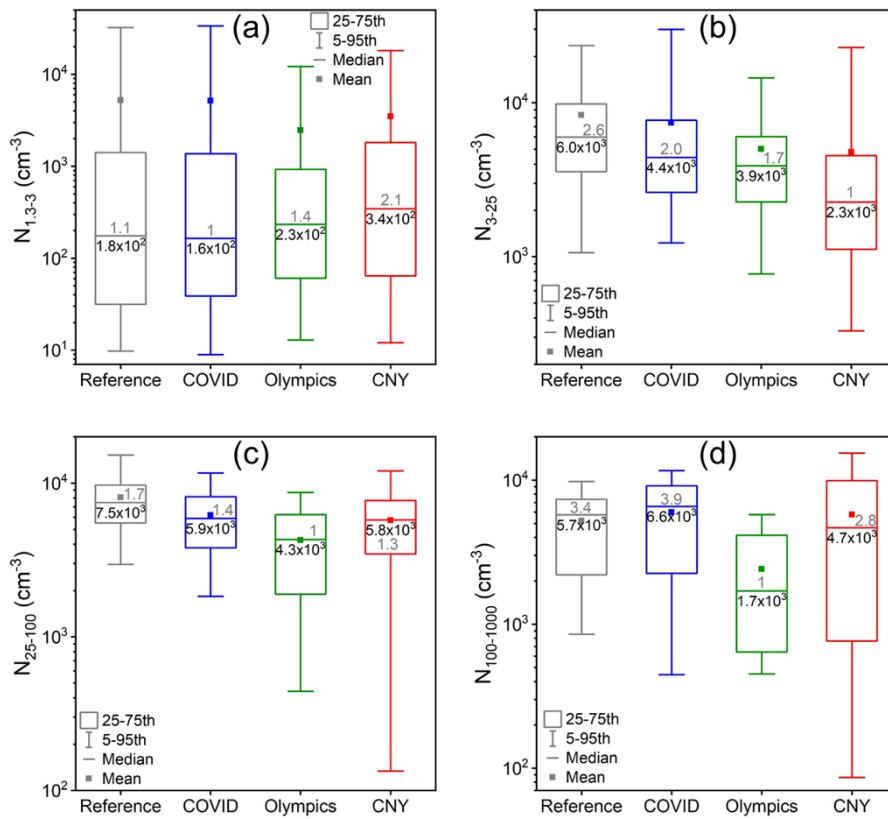
Figure 16. Comparisons of number concentration of (a) sub-3 nm particles ($N_{1.3-3}$), (b) 3-25 nm particles (N_{3-25}), (c) 25-100 nm particles (N_{25-100}) and (d) 100-1000 nm particles ($N_{100-1000}$) for reference, COVID, Olympics and CNY periods. The black value inside each box is the median value of corresponding parameter. The gray values are the normalized median values to the lowest median value in each subplot, which is used for quantitative variation comparison between different parameters.
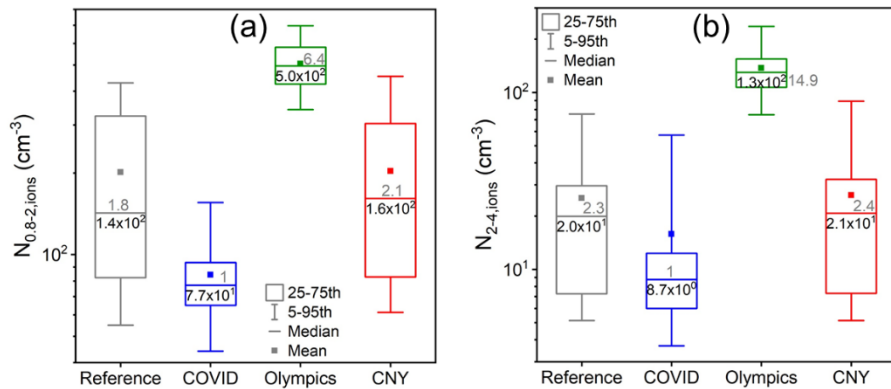
Figure 17. Comparisons of number concentration of (a) 0.8-2 nm ($N_{0.8-2}$) and (b) 2-4 nm positive ions (N_{2-4}) for reference, COVID, Olympics and CNY periods. The black value inside each box is the median value of corresponding parameter. The gray values are the normalized median values to the lowest median value in each subplot, which is used for quantitative variation comparison between different parameters.
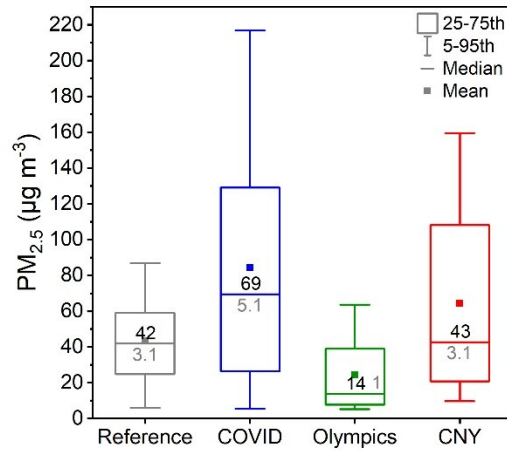
Figure 18. PM$_{2.5}$ mass concentration for reference, COVID, Olympics and CNY periods. The black value inside each box is the median value of corresponding parameter. The gray values are the normalized median values to the lowest median value in each subplot, which is used for quantitative variation comparison between different parameters.
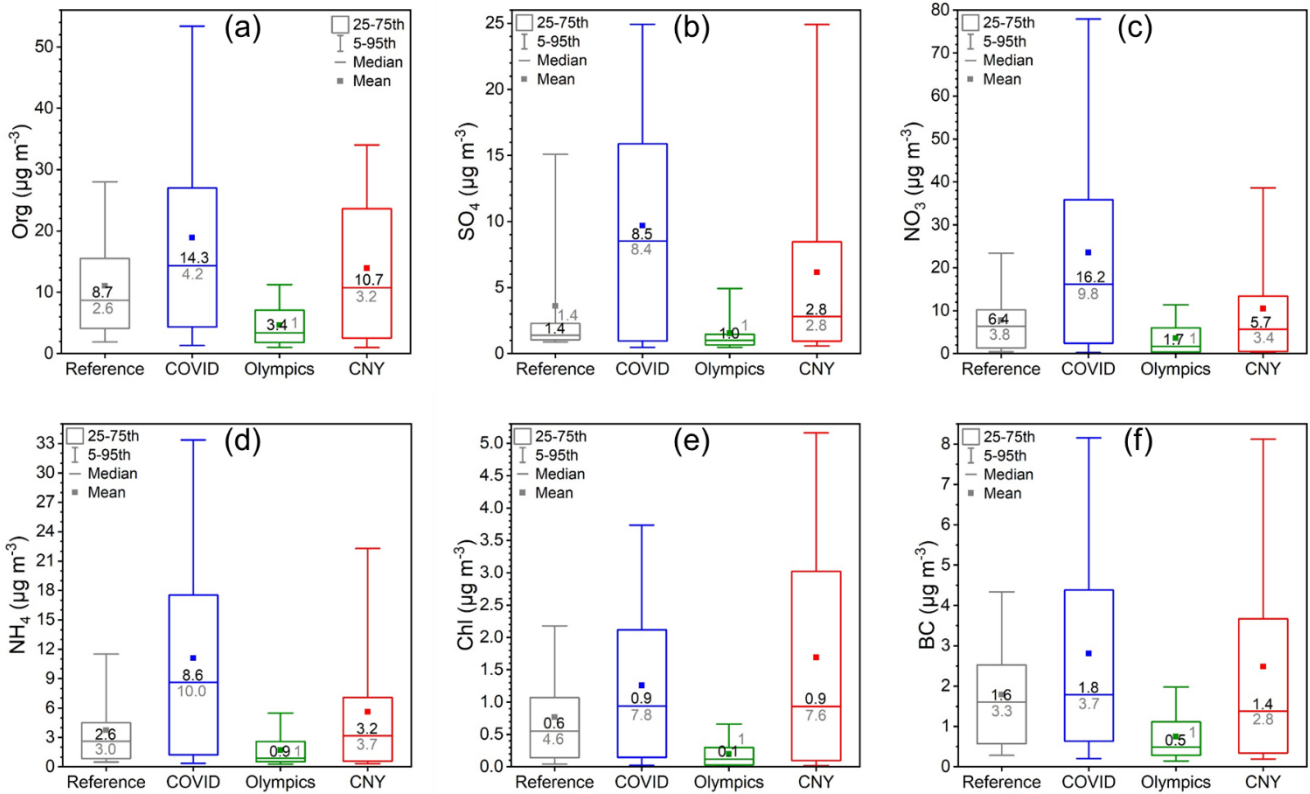
Figure 19. Mass concentrations of PM$_{2.5}$ compositions including (a) organics (Org), (b) sulfate (SO$_4$), (c) nitrate (NO$_3$), (d) ammonium (NH$_4$), (e) chloride (Chl), and (f) black carbon (BC) for reference, COVID, Olympics and CNY periods. The black value inside each box is the median value of corresponding parameter. The gray values are the normalized median values to the lowest median value in each subplot, which is used for quantitative variation comparison between different parameters.
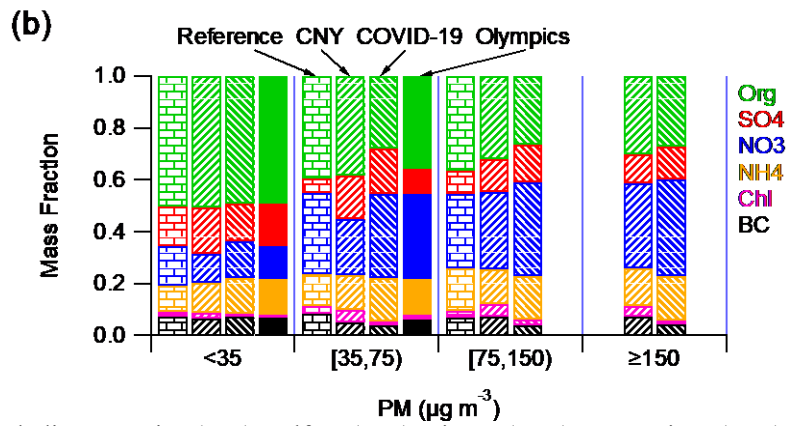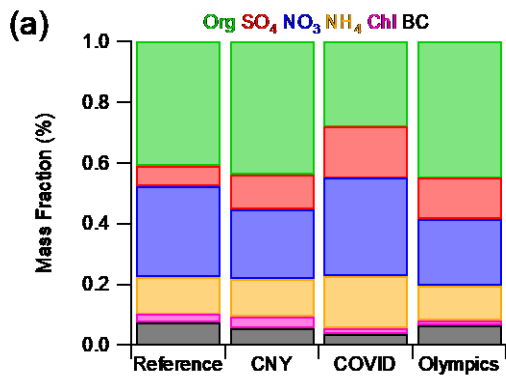
Figure 20. Contributions of PM$_{2.5}$ compositions including organics (Org), sulfate (SO$_4$), nitrate (NO$_3$), ammonium (NH$_4$), chloride (Chl), and black carbon (BC) (a) for reference, COVID, Olympics and CNY periods, and (b) under different PM$_{2.5}$ levels.